Heliyon 10 (2024) e25276

Contents lists available at ScienceDirect

Heliyon

journal homepage: www.cell.com/heliyon

Review article

Prognosis methods of stress corrosion cracking under harsh environmental conditions

Hasan Hamdan [a], Abdullah Alsit [a], Aghyad B. Al Tahhan [a], Omer Mughieda [b], Abdel-Hamid I. Mourad [c], Mutasem A. Shehadeh [d], Mohammad Alkhedher [a,*]

[a] Department of Mechanical and Industrial Engineering, Abu Dhabi University, Abu Dhabi, PO 59911, United Arab Emirates
[b] Department of Civil Engineering, Abu Dhabi University, Abu Dhabi, PO 59911, United Arab Emirates
[c] Department of Mechanical Engineering, United Arab Emirates University, Al-Ain, P.O. Box 17555, United Arab Emirates
[d] Department of Mechanical Engineering, Alfaisal University, Riyadh, P.O. Box 50927, Kingdom of Saudi Arabia

ARTICLE INFO

Keywords:
SCC
Artificial intelligence
Machine learning
Electrochemical testing
Slow strain rate
Ultrasonic testing

ABSTRACT

Stress corrosion cracking (SCC) under harsh environmental conditions still poses a significant challenge, despite extensive research efforts. The intricate interplay among mechanical, chemical, and electrochemical factors hinders the accurate prognosis of material degradation and remaining service life. Furthermore, the demand for real-time monitoring and early detection of SCC defects adds further complexity to the prognostication process. Therefore, there is an urgent need for comprehensive review papers that consolidate current knowledge and advancements in prognosis methods. Such reviews would facilitate a better understanding and resolution of the challenges associated with SCC under harsh environmental conditions. This work aims to provide a comprehensive overview of various prognosis methods utilized for the assessment and prediction of SCC in such environments. The paper will delve into the following sections: exacerbating harsh environmental conditions, non-destructive testing (NDT) techniques, electrochemical techniques, numerical modeling, and machine learning. This review is inclined to serve as a valuable resource for researchers and practitioners working in the field, facilitating the development of effective strategies to mitigate SCC and ensure the integrity and reliability of materials operating in challenging environments. Despite considerable research, stress corrosion cracking in harsh environments remains a critical issue, complicated by the interplay of mechanical, chemical, and electrochemical factors. This review aims to consolidate current prognosis methods, including non-destructive testing, electrochemical techniques, numerical modeling, and machine learning. Key findings indicate that while traditional methods offer limited reliability, emerging computational approaches show promise for real-time, accurate predictions. The paper also briefly discusses notable SCC failure cases to underscore the urgency for improved prognosis techniques. This work aspires to fill knowledge gaps and serve as a resource for developing effective SCC mitigation strategies, thereby ensuring material integrity in challenging operational conditions.

1. Introduction

Stress corrosion cracking is a kind of corrosion that occurs when a material is subjected to both applied load and corrosive

* Corresponding author.
E-mail address: mohammad.alkhedher@adu.ac.ae (M. Alkhedher).

https://doi.org/10.1016/j.heliyon.2024.e25276
Received 6 October 2023; Received in revised form 4 January 2024; Accepted 24 January 2024
Available online 1 February 2024

environments [1]. It is a widespread issue in several areas, especially oil and gas, nuclear power, and aerospace. SCC occurs when a material operating in a corrosive environment is subjected to tensile loading [2], The combined effect of these two elements might cause material degradation and eventually fracture [3]. Numerous factors can lead to SCC, including the composition and concentration of the corrosive medium, the temperature and humidity of the surroundings, the material type, and the existence of other elements that can influence the material's susceptibility to corrosion, like metallurgical flaws or stress concentrations [4]. SCC is one of the most common yet problematic engineering fracture and failure processes [5,6] that is manifested by corrosion fatigue (CF) and hydrogen-induced cracking (HIC). Harsh environments such as high temperature, high salinity, or exposure to aggressive chemicals pose significant challenges to the durability and safety of structural components in various industries, including aerospace, oil and gas, and nuclear power [7,8]. The accurate and timely prognosis of SCC under such harsh environmental conditions is of paramount importance to prevent catastrophic failures and ensure the reliability and longevity of critical assets [9]. Prognosis methods, including both experimental and computational techniques, play a crucial role in assessing the severity and predicting the remaining life of materials affected by SCC [10]. Despite extensive research efforts, the prognosis of SCC remains a significant challenge. The complex interactions between mechanical, chemical, and electrochemical factors make it difficult to accurately assess the severity and predict the remaining life of materials. Moreover, the need for real-time monitoring and early detection of SCC defects further complicates the prognosis process. Therefore, there is a critical need for comprehensive reviews that consolidate the current knowledge and advancements in prognosis methods, enabling researchers and practitioners to better understand and address the challenges associated with SCC. This review paper aims to provide a comprehensive overview of various prognosis methods employed for the assessment and prediction of SCC under harsh environmental conditions. The paper will focus on the following topics: Harsh environmental conditions that exacerbate SCC, Non-Destructive Testing (NDT) Techniques, Electrochemical Techniques, Numerical Modeling, and Machine Learning.

2. Harsh environmental conditions that exacerbate SCC

SCC is a phenomenon that results in the initiation and growth of cracks in metallic materials under specific environmental conditions [11]. The conditions that can exacerbate SCC are often harsh and change from one environment to another, and include factors such as corrosion, vibration, diffusion, mechanical shock, and low-cycle strain hardening [12]. Additionally, cyclical thermal stresses induced by differences in the Coefficient of Thermal Expansion between different interfaces can also contribute to SCC. Structural materials that are more susceptible to SCC include high-strength alloys such as stainless steel and aluminum [13]. Fig. 1 shows an overall diagram of factors that affect SCC under Harsh Environmental conditions.

2.1. Environmental factors

One of the harsh environmental conditions that can exacerbate SCC is high temperature. In high-temperature environments, materials can become more susceptible to SCC due to thermal stresses and the accelerated corrosion processes that occur at elevated temperatures [14]. High-temperature SCC can be a significant problem in industries such as nuclear power generation, where materials are exposed to high temperatures and radiation [15]. Another harsh environmental condition that can exacerbate SCC is exposure to harsh chemicals. Chemicals such as acids, alkalis, and salts can accelerate the corrosion process and increase the likelihood of SCC [9,16]. This is particularly true in environments where these chemicals are present in high concentrations, such as in the chemical processing industry [17]. Other factors that can also contribute to SCC include high pressure, irradiation, and high humidity [18]. In high-pressure environments, materials can experience higher levels of stress, which can increase the prospect of SCC [19]. This is particularly true in the oil and gas industry, where materials are subjected to high-pressure environments during drilling and production operations [20]. Radiation exposure can also exacerbate SCC. In environments with high humidity or moisture, materials can be exposed to a corrosive environment that can accelerate the corrosion process and increase the probability of SCC. This is particularly true in industries such as marine and offshore oil and gas, where materials are exposed to saltwater and high humidity [21,

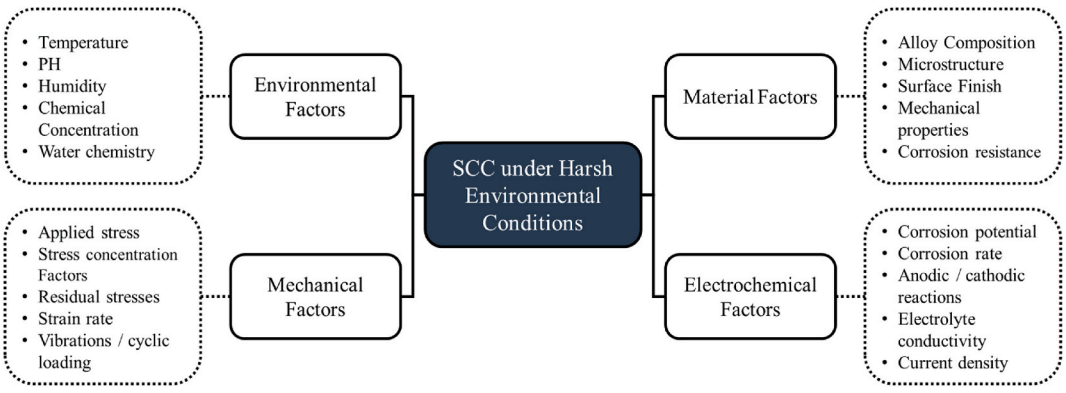

Fig. 1. Factors that exacerbate stress corrosion cracking under harsh environment conditions.

22]. The factors that influence the corrosion of buried natural gas and oil pipelines include the Chemical composition of the soil, including pH levels, moisture content, oxygen concentration, etc. [23]. Also, Temperature fluctuations in the environment can cause thermal fatigue on pipeline materials leading to cracking or other forms of damage [24]. The presence of corrosive chemicals such as acids or alkalis is present in soils due to industrial activities nearby [25]. Bacterial activity, or Microbiologically Induced Corrosion (MIC), causes localized pitting corrosion damages on external surfaces resulting in loss of wall section thicknesses over time [26].

2.2. Mechanical factors

SCC occurs under tensile mechanical or thermal loading, and it is affected by several mechanical factors that can aggravate the severity of cracking, especially in harsh environmental conditions [27]. These mechanical factors include applied stress, stress concentration factors, residual stress, strain rate, vibrations, and cyclic loading [28,29]. The presence of stress concentration factors and residual stress can further promote the propagation of stress corrosion cracks by deteriorating the local mechanical properties of materials [30]. In addition to these factors, strain rates play a fundamental role in promoting stress corrosion cracking by lowering the threshold for crack propagation [31]. Moreover, vibrations and cyclic loading can also contribute to the deterioration of material properties by inducing intergranular corrosion penetration and reducing crack closure stresses [32]. It is important to consider these mechanical factors when dealing with materials under tensile loading and corrosive environments, as ignoring them could lead to catastrophic failure.

2.3. Material factors

Research has shown that the stress intensity factor K_1 is a significant indicator characterizing the stress corrosion process in metals [33]. Corrosion cracking can typically cause ductile metal alloys subjected to high temperature and tensile stress to fail suddenly [34]. Ultrahigh-strength steels are particularly susceptible to stress corrosion cracking in aqueous solutions [35]. According to Banda, three types of corrosion have been explained, with stress corrosion cracking occurring when high mechanical stress is present in a corrosive environment, causing failure of metallic materials by cracking [36]. To evaluate the stress corrosion cracking resistance of metallic alloys, fracture mechanics principles, and pre-cracked specimens have been used successfully in recent years [37]. These pre-cracked specimens can be produced by fatigue, which creates compressive residual stresses in the vicinity of the crack tip [38]. In addition, Li has pointed out that stress-corrosion cracking occurs when the corrosion product occupies a larger volume than the volume of metal destroyed [39]. Combined with the applied stress and the stress from the wedging action of the corrosion product, this can be significant enough to propagate a crack [40]. Furthermore, it is crucial to consider factors such as alloy composition, microstructure, surface finish, mechanical properties, and corrosion resistance when designing materials that will be exposed to extreme environmental conditions, as these factors can exacerbate stress corrosion cracking [41].

2.4. Electrochemical factors

Several electrochemical factors exacerbate stress corrosion cracking under extreme environmental conditions, including the metal's corrosion potential, corrosion rate, Anodic and cathodic reactions, electrolyte conductivity, and current density [42]. These factors play a crucial role in the initiation and propagation of stress corrosion cracking. In extreme environmental conditions, the corrosion potential can shift towards more aggressive values, thereby increasing the susceptibility to SCC [43]. For instance, highly positive potentials (more oxidizing) can promote anodic reactions, while highly negative potentials (more reducing) can favor cathodic reactions, both of which can exacerbate the SCC process [44]. The corrosion rate tends to escalate, leading to enhanced metal loss and weakening of the material. The accelerated corrosion rate can provide more active sites for crack initiation and propagation [45]. The anodic and cathodic reactions occurring at the metal surface directly influence SCC behavior. Under extreme environmental conditions, the presence of aggressive species, such as chlorides or sulfides, can promote localized anodic dissolution of the metal, generating corrosive reaction products [46]. Electrolyte conductivity affects the transport of ions and charge transfer processes, influencing the overall electrochemical behavior and SCC susceptibility [47]. High electrolyte conductivity facilitates the movement of corrosive species toward the metal surface and enhances the ionic flow, leading to a higher likelihood of SCC initiation and propagation [48]. Higher current densities can result from increased anodic dissolution or cathodic processes. Elevated current densities can accelerate localized corrosion and promote crack growth by providing the necessary electrochemical conditions for SCC [49].

Methods for prognosis of SCC under harsh environmental conditions.

3. Non-destructive testing (NDT) techniques

3.1. Ultrasonic testing

To test for the stress corrosion cracking (SCC) failure of materials, one can go through experimental destructive testing, as in constant slow strain rate testing (SSRT), constant load testing, and constant total strain testing [50], in which the specimen is destroyed and failed to collect SCC data. However, non-destructive testing (NDT) methods are widely used to test components for SCC in a material. NDT can be done through Ultrasonic testing, Radiography, Eddy Current testing, DCPD testing, and many other methods [51]. The ultrasonic test method is a nondestructive test methodology that uses high-frequency sound waves to detect material flaws and defects [51–53]. This is done by sending ultrasonic waves, from the transmitter part of the sensor, through the material and

measuring the time needed for the waves to be reflected and travels back to the receiver of the sensor, and the different peaks and dibs of the sound wave are translated into, cracks, pits, defects, or a normal smooth surface.

3.1.1. Through transmission

Through transmission is an ultrasonic testing method in which the internal structure of the material is thoroughly tested, as described and shown by Fig. 2, where two transducers are placed on two opposite sides of the material and ultrasonic waves are sent through it, from one transducer to another Any detected change in the recorded waves by the receiver indicates a defect within the material, allowing this method to be the choice for materials with access difficulties and irregular geometries [54–57]. This method has been thoroughly utilized in many engineering test disciplines, including civil and mechanical applications. For SCC, this method is conducted in pipelines, in which access to the inside is deemed to be difficult [58], and these pipelines are noted to be under continuous corrosive conditions, with some transporting highly toxic chemicals, such as H_2S, which is a main chemical byproduct in the oil and gas industry.

3.1.2. Pulse echo

Pulse echo testing is another non-destructive testing type that falls under the ultrasonic test methodology. It works by sending short bursts of ultrasonic high-frequency waves into a material using a transducer that acts as both the transmitter and receiver, and when the waves encounter a defect, a change is noted in the wave, and it is then reflected to the same transducer, which will now act as a receiver [59–62]. This method can be performed in different modes such as the contact testing methodology [63], in which the material is directly in contact with the transducer, and immersion testing [64], in which the material or test object is submerged in a water tank to facilitate the ultrasonic tests. This method can be applied to materials that are both under atmospheric and submerged harsh corrosive conditions, which allow for remote and continuous material testing to detect SCC material defects [65]. Fig. 3 shows a three-experiment setup done to measure the relative fraction of gas, liquid, and solid inside pipe runs of a biogas plant, using an ultrasonic sensor in pulse-echo mode, and at three different angles (top position, air-water phase boundary, and 90° from the top position), this research is done by Mukherjee et al. [66], representing a novel method to detect segregated phases in digesters of biogas plants.

3.1.3. Resonance

Resonance-based ultrasonic testing is like the pulse-echo type, however, the difference lies in the transmission regularity, which can be adjusted in this case, and the application of the transducer, where it can be used when only one side of the specimen or material is accessible, which is quite useful in the case of structural inspections, especially in pipelines [67,68]. Shown in Fig. 4 is a test setup used to determine the dynamic Young's modulus of a specimen using a lead zirconate titanate (PZT) ultrasonic transducer and a laser doppler vibrometry (LDV) to map the resonant ultrasound waves, this study done by Jung et al. [69] shows that the mechanical properties of materials can be enhanced and studied using ultrasonic fatigue testing methods, which contribute to better enhancing the design of specimens and components.

3.2. Radiography

Radiography is a non-destructive testing type that works on the principle of radiation, in which radiation particles and isotopes are emitted from a source, which can typically be x-rays or gamma-rays. The rays are absorbed by digital or traditional film detectors placed on the opposite side of the test specimen or material, which form an image based on the captured radiation particles [70,71]. Digital films form two-dimensional images through the absorbed radiation, while digital detectors for immediate images for the user to see on an interface. The material defects would alter the radiation, which forms discontinuities in the formed image by the detector,

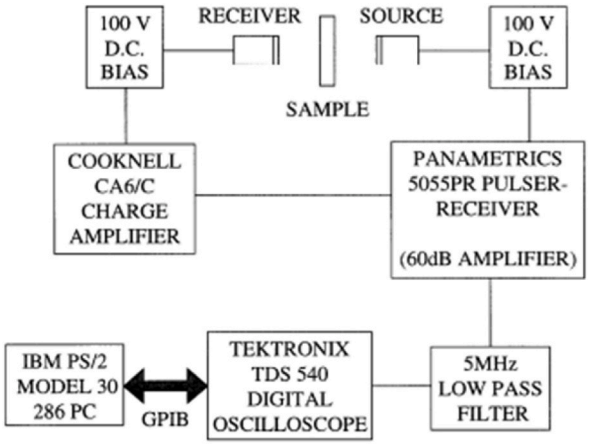

Fig. 2. Schematic of a through-transmission ultrasonic test apparatus [54].

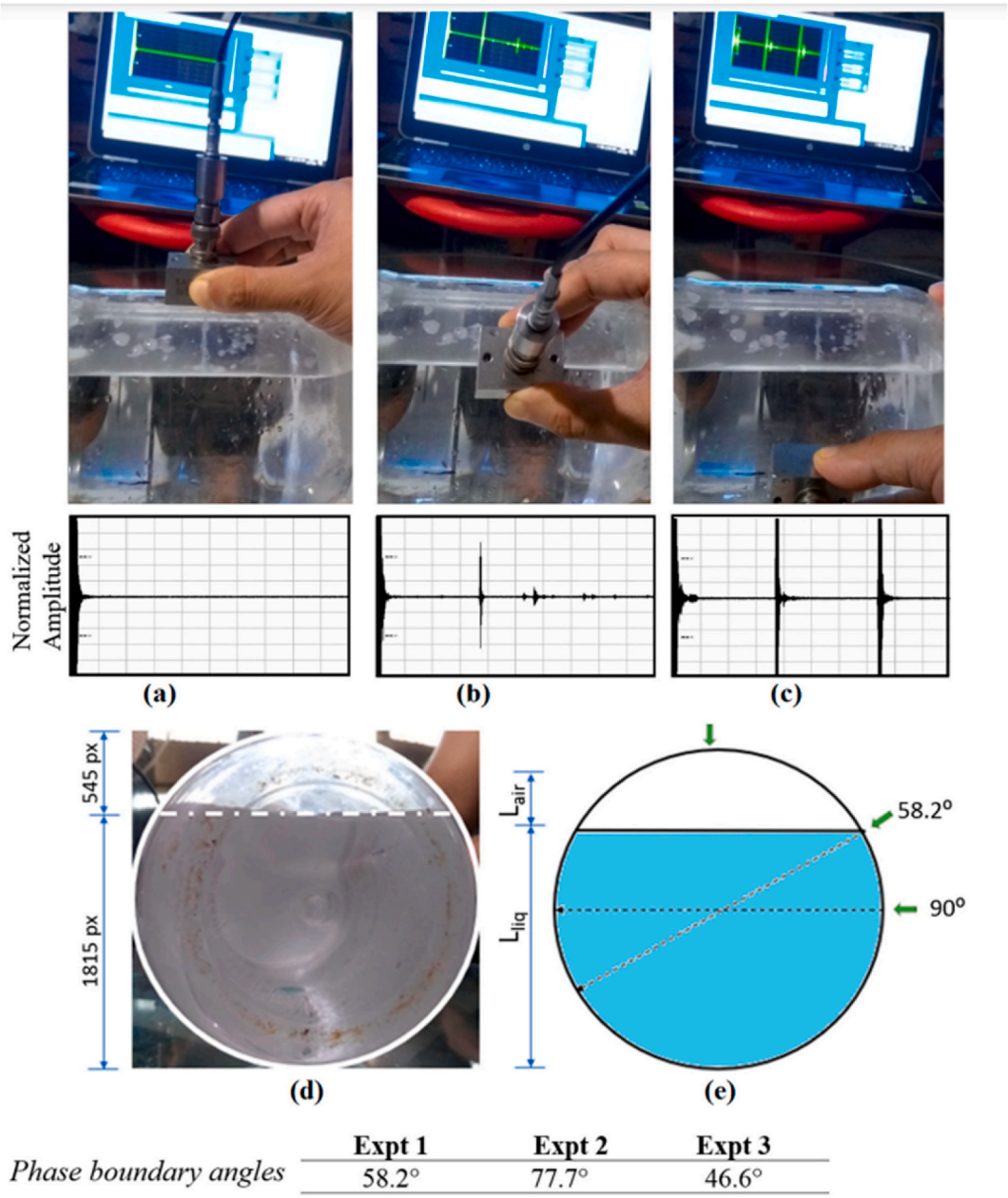

	Expt 1	Expt 2	Expt 3
Phase boundary angles	58.2°	77.7°	46.6°

Fig. 3. Pulse Echo Test of a Two-Phase System in a Biogas Plant Pipe Set up; a) Ultrasonic Sensor Placed on the Top Position of the Pipe, b) Sensor is Placed on the Water-Air Phase Boundary Position, c) Sensor is Placed 90° From the Top Position, d) Photograph of Experiment 1, and e) Phase Composition Estimation Based on the Critical Angles Observed During the Sensor Sweep. This study is done by Mukherjee et al. [66].

and this is where the trained users would classify the material defects and irregularities, through the image discontinuities [72]. When dealing with this type of testing methodology, extra caution must be taken due to the presence of radiation, which can be done by using proper protective equipment and careful test execution. As discussed, there are two main types of radiography test methodologies, one is the conventional type, which is also known as film radiography, and the other is called digital radiography. Digital radiography is also divided into two different types, one is Computed Radiography (CR), which works by using phosphorus-coated reusable plates that capture the transmitted radiation energy, and the plates are then laser scanned to produce images, and the other type is called Direct Radiography (DR), which uses solid-state detectors to directly capture the radiation and produce images [73]. Fig. 5 shows a sample of X-ray images taken of a weld cross-section, where Fig. 5a shows the X-ray image obtained for the defects detected, and Fig. 5b shows the LP results that are obtained using dye penetrant testing.

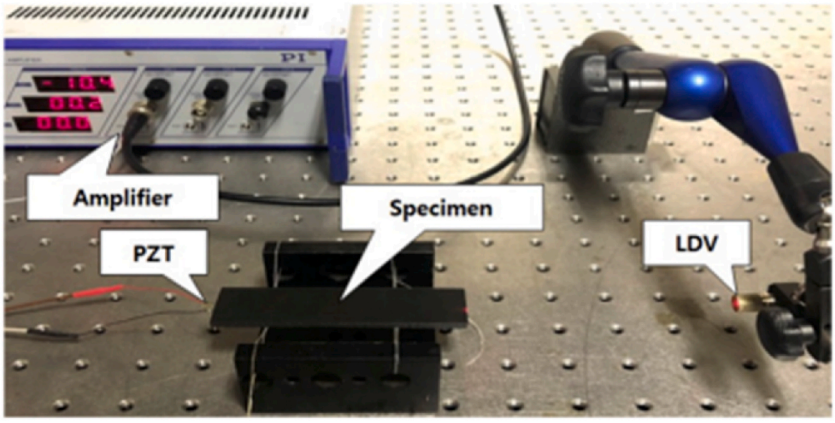

Fig. 4. Measurement of the Dynamic Young's Modulus using the Resonance Ultrasonic Testing Technique [69].

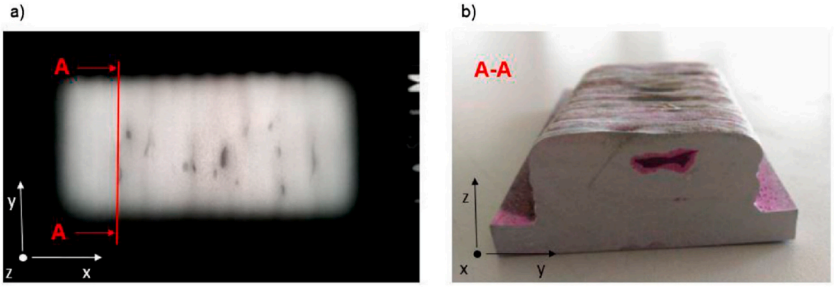

Fig. 5. X-ray and LP Comparison of Defect Detection, a) X-ray results, and b) LP results [70].

3.3. Eddy current testing

Eddy current testing is another non-destructive method to assess the quality of conductive materials. Its working principle, as described in Fig. 6, is based on inducing electric currents, in which a coil or a probe is placed near the surface of the test material and an alternating current is passed through it, which produces a changing magnetic field, and induces eddy currents [74]. The interaction between the eddy currents and the material being inspected generates a secondary magnetic field, and any variations in this field are a result of material defects and discontinuities. Eddy current testing methodologies include the first type known as surface eddy current testing, which works by scanning the surface of the material in the same way as the described working principle, and this type is the most basic type of eddy current tests [75]. The tubular eddy current testing is used to inspect conductive tubes by moving a coil or probe through the interior of the test tube [76]. The third type is the weld eddy current testing, which is specifically designed to test welds and study the weld defects [77]. The fourth type is the array eddy current testing, which works by utilizing an array of probes to inspect a larger area simultaneously [78]. The fifth type is the remote field testing, which is used to inspect conductive tubes by inducing currents on the external and internal surface of the tube to penetrate the walls allowing for the detection of defects at multiple depths [79]. The sixth and final type is the pulsed eddy current testing, which works by sending short electromagnetic pulses into the material and then measuring the response signals, which is done to assess the thickness and corrosion under the insulation of metal

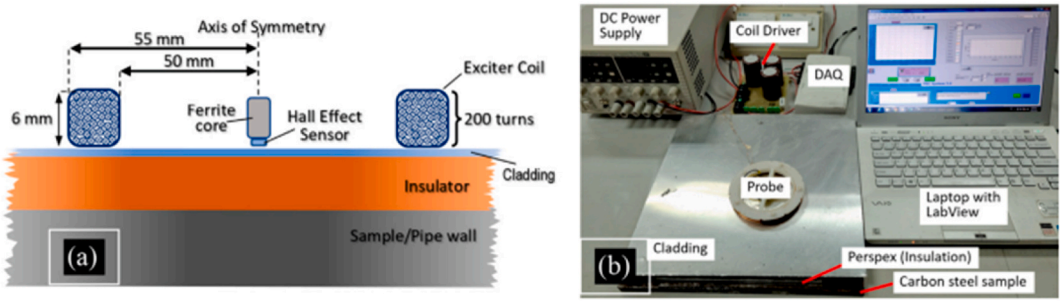

Fig. 6. (a) Cross-section illustration of an eddy current testing experimental setup, (b) image of the actual experimental setup [80].

parts [80].

3.4. DCPD

The Direct Current Potential Drop (DCPD) technique is a non-destructive testing method that works based on the change in potential around material discontinuities. It is a non-destructive method that is mainly used in SCC or fatigue cracking defects. It is generally made of a pair of electric potential sensors placed on opposite sides of the specimen being studied, as shown in Fig. 7, and around the region of interest, and a low-level direct current is applied through the structure, where the electric potential is measured, and any crack or discontinuity in the material will show a drop in the measured potential [81–83]. It is based on the principle that cracks in the material would act as a resistor in an electric circuit, whereas the crack propagates, the resistance increases causing the potential readings to change and drop, which would allow for the direct calibration of the potential drop readings to the instantaneous crack length, and the crack propagation rate [84].

Table 1 shows a comparison of recent works for the prognosis and prediction of SCC using NDT methods, including the cases studied, and the results obtained. Although NDT methods are commonly used for SCC failure detection and in most cases prediction as well, we can note that they require skilled personnel to operate them, understand how they are used, and understand the output data they provide. Thus, in most cases, they are noted as an expensive method of predicting or detecting SCC in pipelines and mechanical components.

4. Electrochemical techniques

4.1. Electrochemical impedance spectroscopy

Corrosion is an electrochemical process in basic terms. Any material or part of interest works in an environment condition that causes a certain amount of corrosion, and corrosion is an oxidation and reduction reaction that happens between the environment and the part that is working inside of it, which is a process of exchange of particles and electrons [90]. Thus, to study the corrosion of any material, the electrochemical properties of the system must be investigated, and two main techniques are employed. The first method is called the Electrochemical Impedance Spectroscopy (EIS) technique, and the second method is called the Potentiodynamic Polarization technique.

Electrochemical impedance spectroscopy is an electrochemical technique that studies the surface of a material. EIS works by applying a small amplitude of an alternating current (AC) signal to the electrochemical system and measuring the voltage response, where the signal applied is typically sinusoidal and varied over a range of frequencies, and then the impedance response of the system is determined [91]. The obtained system impedance is then used to generate a spectrum or plot, and two main plots used to analyze the generated spectrum are called the Bode and Nyquist plots.

4.1.1. Bode plot

The Bode plot is a combination of two plots in one, where the horizontal x-axis is the logarithmic scale of the frequency, the first vertical y-axis is the logarithm of the impedance, and the second vertical y-axis is the phase shift [92]. The first plot is called the magnitude plot, in which the magnitude of the response of the system is represented as the logarithm of the amplitude as a function of the frequency, while the second plot is called the phase plot, which represents the phase shift of the system as a function of the frequency.

4.1.2. Nyquist plot

The Nyquist plot is both literally and figuratively more complex than the bode plot. The literal part deals with the complex negative impedance as a function of the system's frequency response, where the imaginary reactance of the system's impedance is plotted (vertically) against the real resistance (horizontally) [93]. However, for the figurative part, the Nyquist plot is very complex to deal with and study, it is very sensitive to the changes in the system and would produce different results with slight uncertainties.

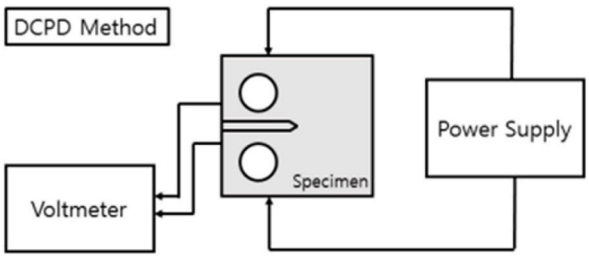

Fig. 7. The DCPD method [84].

Table 1
Comparison of non-destructive technique.

Ref	NDT Method Used	Application for SCC Prognosis	Environment and Material Case	Results Found
Hernandez-Valle et al. (2014) [52]	Ultrasonic NDT	Prediction of SCC Failure and Detection of SCC Defects	AISI 304 Stainless Steel Sections of Pipes	Sonograms of the Defects, with SCC Crack and Pits Found
Cai et al. (2017) [85]	DCPD NDT	Prediction of SCC Defections in Materials Used in Chemical and Nuclear Power Plants	Austenitic stainless steel of type 316 in boiling 42 % MgCl2 solution	Determining Conductivity in SCC Crack Region with Experimental and Numerical Methods
Cai et al. (2020) [86]	Eddy Current and DCPD NDT	Prediction of Conductivity Distribution in a Material due to SCC	three plates of type 316 austenitic stainless steel	ECT and DCPD Results for SCC Conductivity were Shown to be Higher around the Crack tip area
Ooka et al. (2017) [87]	Digital Radiographic NDT	Prediction of Pitting Corrosion Based on a Phase Field Model	Seven Carbon and Stainless-Steel Plates Under Surface, Fatigue, and SCC Conditions	Identification of Material Defects Under Different Conditions
Wang et al. (2019) [88]	DCPD NDT	Monitoring SCC Defects in Steel Alloys	321 Stainless-Steel in a Solution of 0.5 M H2SO4/0.01 M KSCN at room temperature	Crack Propagation and Damage Assessment and Prognosis
Yusa et al. (2007) [89]	Eddy Current NDT	Prediction of SCC Material Failure Under Different Loading Conditions	Six Austenitic Stainless-Steel Plates in MgCl2 Solution at Boiling Temperature	Monitoring the Change in EC Signals due to Change in Load Conditions

4.1.3. *Equivalent circuit fitting*

Equivalent circuit fitting is a technique that is done using the frequency response obtained from the discussed plots and finding a mathematical model or equivalent electric circuit that matches the experimental impedance data, which provides insights and information into the underlying electrochemical process occurring within the system [94–97]. As explained, the electric circuit uses electrical components, which can be a simple resistor, capacitor, or system impedance. In corrosion and SCC studies, there are many different EIS equivalent circuits which, depending on the system of interest, can be a simple metal under corrosion, a metal with coating and corrosive conditions, a disbanding coating with film resistance and corrosion, or other experimental cases. These cases can be studied using an EIS sensor and a spectrum analyzer [98–101]. Cases, circuits, and systems can be represented as mathematical and physical representations. Equation (1) represents the simple resistor in an equivalent circuit, while similarly the capacitor is shown in Equation (2). Fig. 8 shows the generalized Randles equivalent circuit of an electrochemical system. The electrochemical cell is an electric circuit by nature, where the current flows from one electrode to another through the solution and encounters obstacles such as protective layers formed on the electrodes called the double layer, which is represented as a capacitance as in Equation (3).

$$R = \frac{U}{I} \tag{1}$$

$$C = \frac{Q}{E} \tag{2}$$

$$C_{dl} = \frac{1}{R_{et} 2\pi f_{max}} \tag{3}$$

The process inside the electrochemical corrosion cell or any cell is also a diffusive process with mass transport, which is simulated and represented using the Warburg Impedance term in Equation (4), and the diffusion coefficient in Equation (5), which describes the diffusion of ions that occur inside the electrolyte of the electrochemical cell [103].

$$Z_W = \frac{\sigma}{\sqrt{2\pi f}} - j\frac{\sigma}{\sqrt{2\pi f}} \tag{4}$$

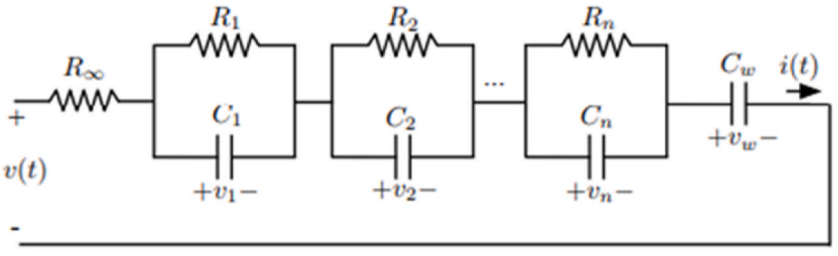

Fig. 8. Generalized randles equivalent circuit of a multicell electrochemical system [102].

$$\sigma = \frac{RT}{Az^2F^2\sqrt{2}}\left(\frac{1}{\sqrt{D_O c_O^b}} + \frac{1}{\sqrt{D_R c_R^b}}\right) \tag{5}$$

Where σ is the Warburg coefficient, R and F are the gas and Faraday constants respectively, D is the diffusion coefficient, c^b is the species' concentration inside the solution, and T is the solution temperature, the sub- R and O indicate the oxidized and reduced species. While in Equation (4), Z_W is the Warburg element impedance.

4.2. Potentiodynamic polarization

Potentiodynamic polarization is an electrochemical technique used in corrosion studies of metallic materials, in which the current response of an electrode is measured as a function of the applied sweep potential [104–106]. As described, in potentiodynamic polarization, a constant rate of potential is swept on the working electrode, which is typically the specimen or material of study, and the sweep is done from a more negative potential to a more positive potential. If the potential sweep is done from a negative (cathodic region) to a positive (anodic region) value manner, the process is called Anodic Polarization, where the anodic dissolution, active dissolution current, and passivation behaviors are studied. On the other hand, if the sweep is done oppositely, the process is then called Cathodic Polarization, in which the hydrogen evolution, oxygen reduction, and cathodic current response are studied and used to assess the material's susceptibility to cathodic reactions (Hydrogen Induced Corrosion) [107,108]. This electrochemical process allows the researcher to obtain the very important Tafel Plot, which correlates the swept potential (swept potential value is against the potential value of the reference electrode) against the recorded logarithmic scale of the current or current density [109]. This plot helps researchers obtain very important data, such as the corrosion potential, corrosion current, corrosion rate, and the current density change over time.

5. Numerical modeling

5.1. SCC mechanisms

Understanding the underlying mechanisms of SCC is crucial for developing effective prevention strategies and ensuring the integrity and safety of critical infrastructure. Over the years, extensive research has been conducted to unravel the intricate processes involved in SCC initiation, propagation, and failure [110–112]. Multiple mechanisms have been proposed, including film rupture, hydrogen embrittlement, surface mobility, and coupled environment fracture. These mechanisms consider factors such as plastic deformation, electrochemical reactions, diffusion, and microstructural characteristics [113]. However, a comprehensive

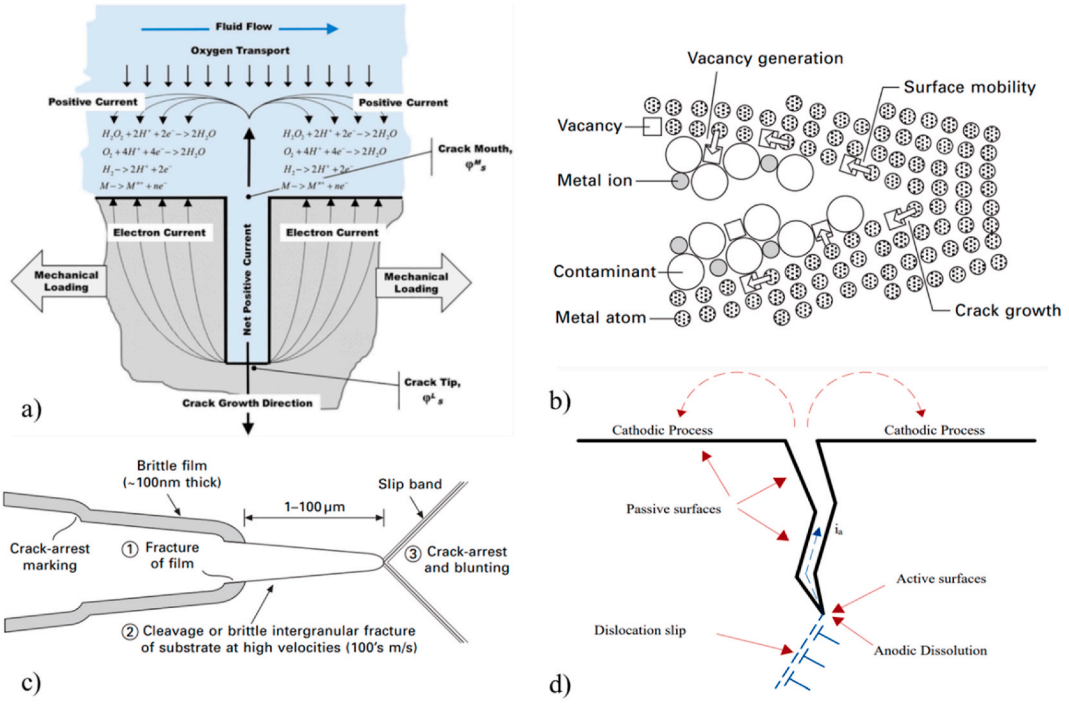

Fig. 9. Types of SCC mechanisms (a) coupled environment fracture model [114] (b) the surface mobility mechanism [115] (c) film-induced cleavage mechanism [115] (d) film rupture dissolution repassivation mechanism [116].

understanding of SCC mechanisms is still evolving, and further investigations are necessary to elucidate the interplay between various factors and advance our knowledge in this field. Fig. 9 indicates various types of SCC mechanisms, including the coupled environment fracture model (Fig. 9a), the surface mobility mechanism (Fig. 9b), the film-induced cleavage mechanism (Fig. 9c), and the film rupture dissolution repassivation mechanism (Fig. 9d).

5.1.1. Film rupture dissolution repassivation model

The mechanism described in the passage has been extensively studied in the context of stress corrosion cracking of alpha brass in an ammoniacal environment and caustic cracking of boiler steel [118]. The model is based on the concept of a strain-induced rupture of a protective film, where plastic strains play a significant role in the failure process [119]. According to the theory, a passivation film exists on the surface of the metal, which serves as protection against corrosive agents [120]. However, mechanical loading can cause plastic strain, leading to the rupture of the passivation film [116]. Once the film is ruptured, the bare metal is exposed to a corrosive environment. This process of disruptive strain (rupturing of the protective film) and film formation (due to repassivation) alternate with each other. Stress corrosion cracking occurs when the rate of rupture of the oxide film is higher than the rate of repassivation of the film [121]. One of the widely used models for SCC is the slip dissolution/film rupture mechanism, which was developed by Ford and Andersen [122,123]. It suggests that crack growth is affected by the strain rate, the charge oxidation density, and the stress intensity factors, which are factors of the crack tip region following Equation (6).

$$v_{ct} = \frac{M}{Z.\rho.F}.\frac{Q_f}{\varepsilon_f}\left(\frac{d\varepsilon}{dt}\right)_{ct} \text{ EQ} \tag{6}$$

where: v_{ct} is the crack tip growth rate, M is the molecular weight of the material, z is the charge of the anodic dissolved material, ρ is the material density, F is the Faraday constant, Q_f is charge density per film rupture event, ε_f is the oxide fracture strain, and $(d\varepsilon/dt)_{ct}$ is the crack tip strain rate. The model's exceptional predictive abilities stem from its foundation in a deep comprehension of the crack advancement mechanism involving film rupture and repassivation.

5.1.2. The surface mobility mechanism model

The surface mobility mechanism (SMM) employs a unique strategy where cracks progress not through anodic dissolution, but through the movement of atomic vacancies formed at the crack edges near the tip. This is the only model that presents equations to forecast the rate at which cracks spread, and it also accounts for the introduction of hydrogen in the process, thereby extending the scope of stress corrosion cracking (SCC) theory to encompass hydrogen embrittlement [124–126]. Rhead [127] demonstrated that contaminants have an impact on surface mobility. Building on these findings, Galvele [128] proposed the surface mobility mechanism for stress corrosion cracking (SCC) based on four hypotheses: (i) The presence of the environment alters the surface self-diffusivity of the metal. (ii) SCC occurs at temperatures lower than 0.5 times the absolute melting temperature. (iii) Only elastic stresses play a significant role in the SCC process. (iv) SCC transpires through the capture of vacancies by the crack tip. Galvele developed Equation (7) to estimate the rate at which cracks propagate (v).

$$= \frac{D_s}{L}\left[\exp\left(\frac{\sigma l^3 + \alpha E_b}{kT}\right) - 1\right] \text{ EQ} \tag{7}$$

where D_s is the surface self-diffusion coefficient; L the vacancy diffusion distance; σ the elastic surface stress at the crack tip; l the size of the atom; α a dimensionless function; E_b hydrogen binding energy; k the Boltzmann constant; and T temperature.

5.1.3. Coupled environment fracture model

The Coupled-Environment Fracture Model (CEFM), developed for evaluating the crack growth rate (CGR) in sensitized Type 304SS exposed to extreme environmental conditions, focuses on the electrochemical, mechanical, and microstructural properties of the system [129]. The CEFM incorporates both mechanical and electrochemical processes and is based on the differential aeration hypothesis (DAH) [130]. It proposes that crack propagation occurs through a modified slip/dissolution/repassivation (SDR) mechanism. Initially, the CEFM assumed that cracks advance through the SDR mechanism. Later, SDR was adjusted to consider the unexpectedly large microfracture dimension and low microfracture frequency by integrating hydrogen-induced cracking (HIC) into the model [131]. The CEFM calculates the CGR in two steps. Firstly, it determines the electrochemical potential (Ecorr or ECP) of the external surface, and then the CGR is estimated [132]. The CGR calculation involves splitting the system environment into the crack-internal and crack-external environments, recognizing that the transport (Nernst-Planck) and potential distribution (Poisson's or Laplace's) equations for both environments are interconnected through common boundary conditions (concentrations and electrostatic potential) at the crack mouth [133]. Finally, as in Equation (8), the CGR is determined using Faraday's law.

$$v = \frac{MI_0}{Z.\rho_m.F.A_{ct}} \text{ EQ} \tag{8}$$

where M is the composition- and oxidation charge-averaged atomic weight of the metal, rm is the metal density, z is the oxidation number, and F is Faraday's constant. A_{ct} is the area at the crack tip over which dissolution occurs immediately upon rupture of the film, and I_0 is Tafel's equation to yield the current averaged over a slip dissolution-repassivation cycle [114].

5.1.4. Internal oxidation model

Scott and Le Calvar [134] proposed a mechanism to explain the intergranular (IG) embrittlement of alloy 600, focusing on the diffusion of oxygen into the metal lattice. They suggested that embrittlement could occur due to the presence of an oxygen atom layer at the grain boundary, the formation of internal oxide (Cr_2O_3), or the creation of gas bubbles (CO/CO_2). Specifically, considering gas bubble formation, they presented an equation (Equation (9)) to estimate the crack growth rate.

$$= \left(\frac{81.kTD_0}{512.\gamma^3 a^2}\right)\left(\frac{\delta N_S}{6\pi z}\right)^{\frac{1}{2}}\sigma_p K_I \text{ EQ} \tag{9}$$

Where k is the Boltzmann constant, T is the absolute temperature, D_o is the grain boundary diffusion coefficient for oxygen, γ is the surface energy, a is the interatomic spacing, δ is the grain boundary thickness, N_s is the surface solubility of oxygen, z the number of sites explored per gas atom jump, σ_p is the yield stress of alloy 600, and K_I is the stress intensity at the crack tip.

5.1.5. Film-induced cleavage mechanism

In 1985, Sieradzki and Newman introduced the film-induced cleavage (FIC) model to explain stress corrosion cracking (SCC) in typically ductile (fcc) materials [135]. According to this model, the process involves several consecutive stages: (i) the development of a brittle film induced by the environment at the crack tips, (ii) rapid fracture of the brittle film, (iii) propagation of brittle fracture into the underlying substrate, and (iv) subsequent crack-arrest and blunting [136]. Consequently, the model predicts that crack growth occurs intermittently, resulting in the presence of crack-arrest markings on fracture surfaces, which are sometimes observed. FIC applies to both transgranular (cleavage-like) and intergranular cracking [137]. It is presumed that crack velocities decrease as cracks extend, either due to occasional emission of dislocations from crack tips or encountering obstacles like slip bands, leading to extensive dislocation activity, ultimately resulting in crack-arrest and blunting. The cleavage-assisted SCC propagation rate, v_c, is given by:

$$v_c = a_0 f_0 \, exp\left(\frac{G_I \Delta A}{kT}\right) \text{ EQ} \tag{10}$$

where a_0 is the balanced atomic distance, f_0 is the basic lattice frequency, G_I is the system energy release rate, ΔA is the area where the crack is propagating, k is the Boltzmann constant, and T is the Kelvin temperature.

5.2. Computational modeling

Several types of computational modeling techniques have been used to study stress corrosion cracking (SCC) in materials. Finite element analysis (FEA) is one of the most widely used techniques, which involves modeling the mechanical stress distribution in the material and its interaction with the corrosive environment [138]. Molecular dynamics (MD) simulation is another technique that can provide atomic-level insights into the SCC process by modeling the behavior of individual atoms and molecules [139]. Continuum mechanics-based models such as the boundary element method (BEM) and the extended finite element method (XFEM) have also been used to simulate the crack propagation behavior in materials subjected to stress and corrosion [140]. Furthermore, multiscale modeling approaches that integrate FEA and MD simulations have emerged as a promising tool to study SCC at different length scales, from the atomic to the macroscopic level [141]. These modeling techniques have been instrumental in providing a better understanding of the SCC phenomenon and facilitating the development of new materials and prevention strategies. Table 2 compares the numerical methods available in the literature. The table summarizes several studies on stress corrosion cracking (SCC) mechanisms and materials. Different numerical methods like XFEM, CZM, Peridynamics, PFM, and MD are used. Materials studied include Alloy 600, Alloy 690, 316L stainless steel, 304 stainless steel, AISI 4135 steel, and Polycrystalline Ni60Cr30Fe10 alloys. Various load conditions, such as constant load, stress intensity factor, strain rate, and tensile strain, are explored. These studies provide insights into

Table 2
Comparison of numerical methods.

Ref	Numerical Method	SCC mechanism	Material Model	Load Condition
Bashir (2020) [142]	XFEM	Anodic dissolution	Alloy 600 under light water reactor at high temperature	Constant Load
Lee (2018) [143]	XFEM	Coupled environment fracture model	Alloy 690 under primary water	The constant stress intensity factor
Sedlak (2019) [144]	CZM	Slip dissolution	316L stainless steel exposed to cold work in primary water condition	Constant Load
Tan (2022) [145]	Peridynamics	Anodic dissolution	304 stainless steel in a simulated atmospheric environment.	Strain Rate
Mai (2016) [146]	PFM	Film rupture dissolution repassivation	304 stainless steel in high purity water	Constant Load
Emilio (2022) [147]	PFM	Hydrogen assisted cracking	AISI 4135 steel under seawater	Slow strain rate
Liu (2021) [148]	MD	Dissolution-precipitation	Polycrystalline Ni60Cr30Fe10 alloys under high-temperature water	Tensile strain of 40 %

SCC in diverse environmental and material settings, contributing to a deeper understanding of corrosion phenomena.

5.2.1. Extended finite element modeling (XFEM)

XFEM is an innovative computational method that combines the advantages of finite element analysis with the capability to explicitly model crack propagation without the need for re-meshing [149]. By enriching the standard finite element mesh with additional degrees of freedom to capture crack growth, XFEM enables accurate simulations of complex crack patterns and crack interactions [150]. Rehmit [142,151,152] investigates the effect of variations in macrostructural properties of Alloy 600 on stress corrosion cracking plastic zone ahead of the crack-tip using the extended finite element method (XFEM). The results show that the plastic zone is affected by stress intensity factors, yield strength, and hardening exponent “n" of the materials. Lee [143] discusses a parametric study on primary water stress corrosion cracking (PWSCC) initiation and propagation of a control rod driving mechanism by using different mesh qualities. The study aims to suggest an XFEM-based representative model for PWSCC initiation and propagation simulation. Lee and Chang [117] propose a method to accurately evaluate the crack growth rate (CGR) of nickel-base alloys, which are susceptible to primary water stress corrosion cracking (PWSCC) in nuclear components. The method uses the extended finite element method and a strain rate damage model and was verified using Alloy 600 and applied to estimate the CGR curve of Alloy 690 [153]. Example results for XFEM SCC crack growth are shown in Fig. 10 below.

5.2.2. Cohesive zone modeling (CZM)

One approach to understanding and predicting SCC is to use cohesive zone modeling (CZM), which is a numerical technique that simulates the fracture process at the microscale [154]. CZM incorporates the material properties, loading conditions, and environmental factors that contribute to SCC and provides insights into crack initiation and propagation [155]. This method has gained popularity in recent years due to its ability to capture the mechanics of crack growth in a realistic and computationally efficient manner [156]. Chen [157] uses a cohesive zone model to study the effects of corrosion product films on anodic dissolution stress corrosion cracking in flat and U-shaped edge-notched specimens. The simulation results show that the thickness, Young’s modulus, and fracture strength of the corrosion product films affect the susceptibility and threshold stress intensity factor of the SCC. Sedlak [158,144] presents a model to simulate intergranular stress corrosion cracking in boiling water reactors. The model includes an adaptive oxide thickness derived from a slip-oxidation and diffusion model, which is updated in every structural iteration to fully couple the fracture properties of the cohesive element. The model results agree with experiments in the literature for changes in stress intensity factor, yield stress representing cold work, and environmental factors such as conductivity and corrosion potential. Unai [159] presents a microstructural intergranular hydrogen environmentally assisted cracking (HEAC) model using a cohesive zone approach in Abaqus. The model was fitted with parameters using in-situ synchrotron tomography observations of crack initiation and propagation during HEAC of AA7449-T7651 and was able to accurately replicate the real HEAC behavior of the aluminum alloy. Raykar [160] proposes a new strategy to study hydrogen-assisted stress corrosion crack growth using a combination of analytical and finite element solutions. The results show improvement over the full finite element approach and provide a relationship between concentration-dependent reduction in cohesive strength and plastic strain rate. Fig. 11 provides a visual representation of the CT specimen modeled for CZM, including mesh and geometry. The mesh was refined close to the crack path, and the cohesive elements were also refined by tying four cohesive elements to the surface of every bulk element along the crack path. To avoid penetration in the crack path, Abaqus surface-to-surface contact formulation was used for the bulk material elements at the crack path.

5.2.3. Phase field modeling (PFM)

In recent years, phase field modeling (PFM) has emerged as a promising computational tool for investigating SCC behavior [161]. PFM is a versatile numerical technique that simulates crack propagation and material degradation at the mesoscale, capturing the evolution of the crack front continuously and diffusely [162]. PFM extends the traditional fracture mechanics approach by incorporating the phase field concept, which describes the local damage and crack propagation as a continuous variable within the material domain. This allows for a more realistic representation of the crack geometry, including crack branching and tortuosity, and the ability to simulate crack nucleation and growth under different loading and environmental conditions [163]. Nguyen [164,165] proposes a

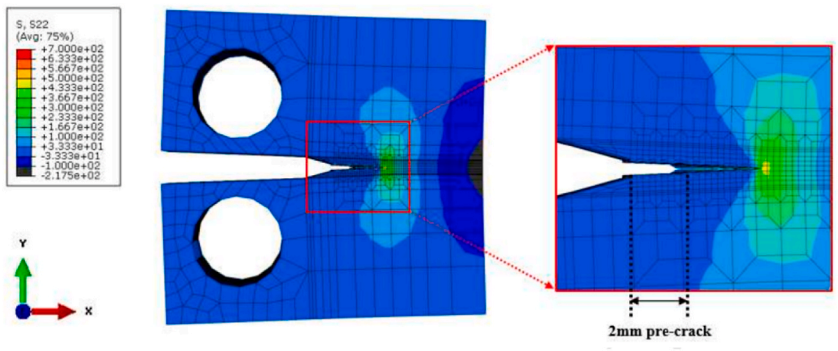

Fig. 10. Example results for XFEM SCC crack growth in Ref. [117], crack shape of alloy 600 in the middle plane at 30 MPa$\sqrt{}$m.

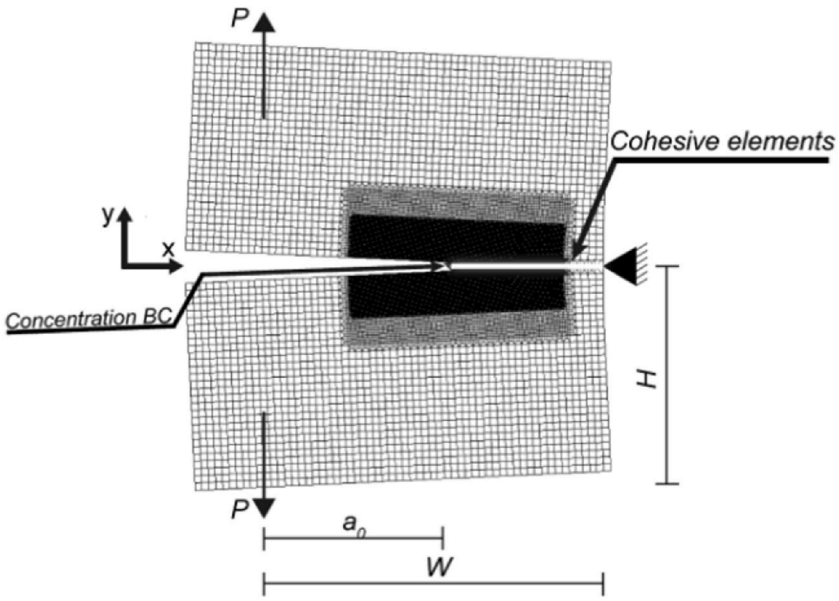

Fig. 11. Czm modeling for ct specimens including the geometry and the mesh model [158].

new model to simulate anodic dissolution induced by stress corrosion fracture growth at the microstructural level. The proposed model is illustrated through several numerical examples involving a full prediction of complex crack network growth induced by stress corrosion cracking within 2D polycrystalline models. The method is applied to an aluminum alloy in a saline medium, allowing for the consideration of both electrochemical and mechanical processes. The numerical results are compared to experimental data obtained by in situ microtomography [146]. presents a new phase field model for simulating stress corrosion cracking (SCC) in metallic materials. The model incorporates the effect of mechanical stresses and investigates the effects of pit morphology, mechanical loading, and the metal microstructure on SCC evolution. Lin [166] proposes a new model to investigate stress-corrosion cracking (SCC) in materials. The model shows that pit-to-crack transition occurs when stress-induced degradation occurs faster than electrochemical dissolution and provides insights into the effect of mechanical loading and initial geometry on promoting SCC. Emilio [147,167,168] This paper presents a new theoretical and numerical framework for modeling mechanically-assisted corrosion in elastic-plastic solids. The model can capture both pitting and stress corrosion cracking, as well as the pit-to-crack transition. Fig. 12 shows two plots providing information on how the initial geometry of the material, mechanical loading, and electrochemical environment affect stress-corrosion

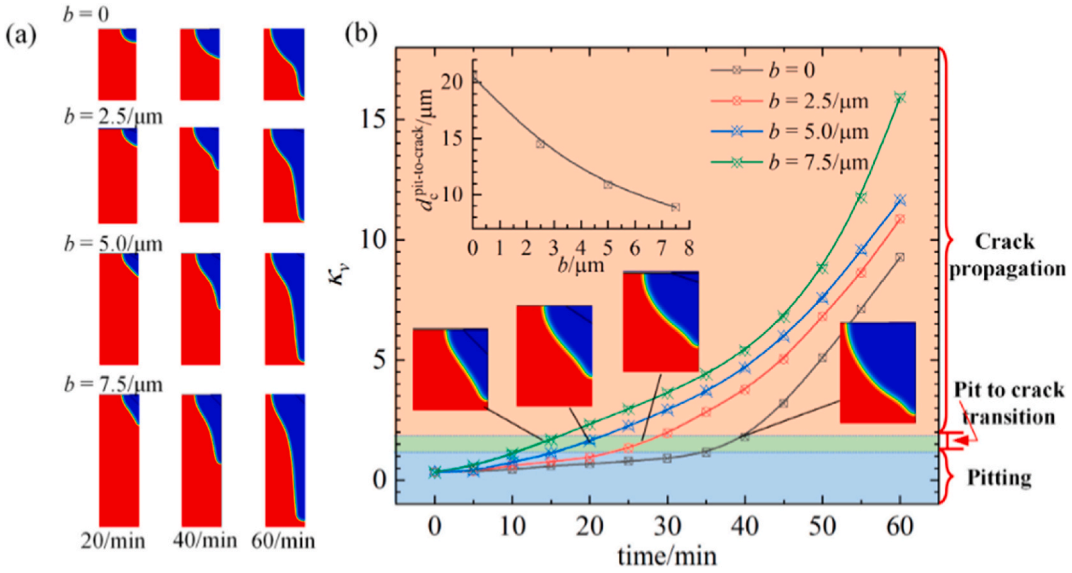

Fig. 12. (a) The Contour Plot of Crack and (b) the Evolution of Variable, κv, with Time for the Samples Subjected to the Traction, Fx = 160/MPa, Having the Different initial pit a = 7.5/μm and b = 0–7.5/μm [166].

cracking. The first plot (Fig. 12a) is a contour plot of a crack, which is a visual representation of the crack's shape and size. The second plot (Fig. 12b) shows the evolution of a variable called κv with time for samples subjected to traction (a force that pulls or stretches the material) of 160 MPa. The samples have different initial pit sizes, with one being 7.5 μm and the other ranging from 0 to 7.5 μm. The variable κv is a relative-rate parameter that characterizes the critical scenario where stress-induced degradation occurs faster than electrochemical dissolution. In simpler terms, it measures the rate at which the material is being degraded due to stress and corrosion.

5.2.4. Peridynamics

The peridynamic model is a non-local and non-linear computational method that can simulate crack propagation and material failure at multiple scales, making it suitable for studying SCC phenomena [169]. Unlike traditional continuum mechanics approaches, the peridynamic model describes the material behavior in terms of interactions between points (or particles) within a material, rather than relying on differential equations. This allows for a more accurate representation of crack initiation, propagation, and branching, as well as the ability to capture the influence of stress fields around the crack tip [170]. Dennj [171] presents a numerical Multiphysics peridynamic framework for modeling adsorbed-hydrogen stress-corrosion cracking (SCC) in a polycrystalline AISI 4340 high-strength low-alloy (HSLA) thin, pre-cracked steel plate. The model is based on the adsorption-induced de-cohesion mechanism and uses microstructural data to simulate the material at the microscopic scale. The results show good agreement with experimental data for crack propagation speed and branching behavior. Shi [172] uses the peridynamics method in corrosion pitting. The simulation is implemented on carbon steel pipes with different corrosion types and loading conditions. The results guide structural design and engineering practice. Moreover, Chen [173] studies pit-to-crack transition problems using the peridynamic model and the extended model considers mechanical damage produced by both corrosion and mechanical strains. Tan [145] proposes an atmospheric stress corrosion model based on peridynamics, which considers the role of hydrogen and stress in anodic-dissolution-dominated stress corrosion cracking. The model characterizes atmospheric corrosion by the change in liquid film thickness on the metal surface in the atmospheric environment.

5.2.5. Molecular dynamics (MD)

To gain insights into the underlying mechanisms of SCC at the atomic level, molecular dynamics (MD) simulations have emerged as a powerful computational tool [174]. MD is a simulation technique that models the behavior of atoms and molecules based on their interactions, allowing for the study of materials at the atomic scale [175]. In recent years, MD simulations have been extensively used to investigate the initiation, propagation, and interactions of cracks in materials under corrosive environments, providing valuable insights into the fundamental processes that govern SCC. MD simulations can capture the dynamic behavior of atoms, including bond breaking and formation, as well as the effect of stress fields around the crack tip [176]. Zhang [177] uses molecular dynamics simulations to study the stress corrosion process of strained a-quartz in liquid water. The results suggest that crack growth is primarily induced by the hydrolysis of strained SiAO bonds located at the crack tip. However, Liu [148] modeled reactive molecular dynamics simulations to study the atomistic initiation of stress corrosion cracking (SCC) of Alloy 690. The study explores the impact of cold work, tensile strain, and grain boundary structures on SCC initiation behaviors. Moreover, Elapolu [178] uses MD simulations to study the subcritical crack growth of graphene in the presence of oxygen molecules. The study investigates the mechanism of environment-assisted cracking of graphene occurring as an interplay between mechanical loading and chemical reactions. Das [179] simulates quantum chemical molecular dynamics to study the oxidation of bare Fe and Fe–Cr surfaces with strain in high-temperature

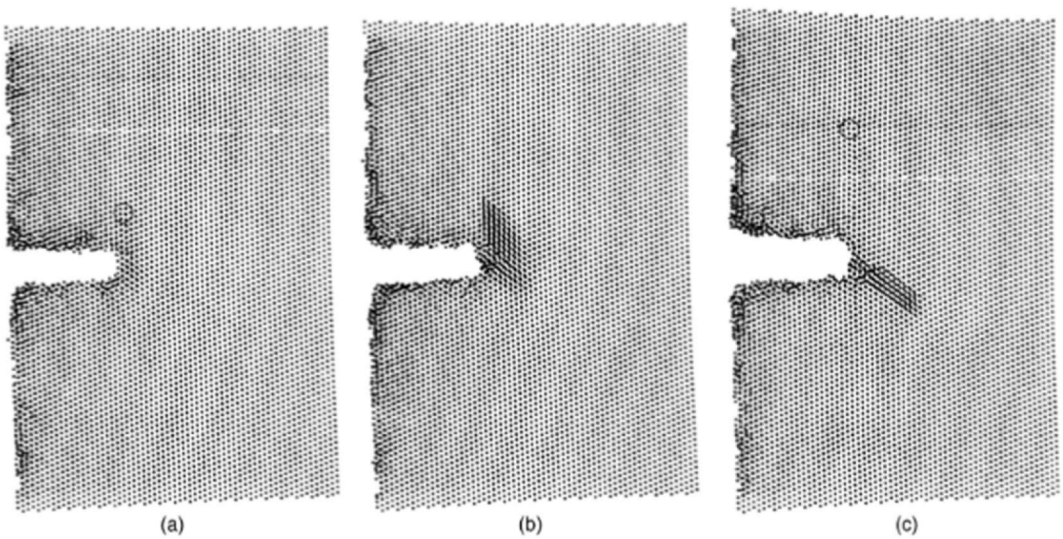

Fig. 13. Describes the Process of Dislocation Emission and Crack Propagation Shows Three Stages of the Process: (a) When the Stress Intensity is 0.58 MPa m1/2, (b) When the Stress Intensity is 0.74 MPa m1/2, (c) When the Stress Intensity is 1.0 MPa m1/2.

water. The results show that the surface morphologies differ between Fe and Fe–Cr due to the strong bond between oxygen and chromium atoms.

Fig. 13 describes the process of dislocation emission and crack propagation in a Cu3Au crystal with a dealloyed layer under mode I loading. The figure shows three stages of the process (Fig. 13a): when the stress intensity is 0.58 MPa m1/2, the first edge dislocation is emitted (Fig. 13b); when the stress intensity is 0.74 MPa m1/2, large amounts of screw dislocations are emitted (Fig. 13c); when the stress intensity is 1.0 MPa m1/2, the crack begins to propagate.

Table 2 below offers a comprehensive survey of simulation methods applied to diverse alloys and environmental conditions, thereby enriching our understanding of SCC prognosis. However, it's important to note that the reliability and accuracy of these models may be compromised due to the disparate testing conditions and evaluation metrics employed across the studies. A more uniform testing methodology would facilitate a more reliable and direct comparison of these prognosis methods. Although, these studies offer rich data that can help predict SCC in various cases of different conditions.

5.2.6. *Machine learning*

Machine learning is a technology that helps users and researchers predict future outcomes and results based on past and present patterns. It is a programming technology in which the creator programs a "model" based on a certain structure or architecture to make what is known as an Artificially Intelligent system. The maker would train and teach the model and system on a large set of data, which can be tables, numbers, graphs, or images/videos, and the model would understand that certain future outcomes can happen based on the pattern it notices from the training set. The trained model is then tested on different metrics to ensure that the accuracy of the predictions is as high as possible to avoid false predictions and results. For stress corrosion cracking, machine learning can be used to effectively predict multiple data and parts of the SCC process in its entirety, which can be the prediction of certain mechanical or electrochemical properties and values, the time-to-failure prediction which tells the researcher exactly when the material or part that is being studied would fail, prediction of the cracks in the material and exactly how they will propagate in the future, and many other possibilities. Machine learning is not limited to one type or method, and in the following sections, the different machine learning methodologies are explored.

5.3. *Supervised learning methods*

Supervised learning is a machine learning method in which the algorithm learns from already labeled data to make predictions and decisions [180]. The goal of this algorithm, as evident in Fig. 14, is to train a model that can generalize and provide accurate predictions or classifications for new unseen data based on provided learning examples, thus the process inside this model is a pattern and relationship-finding process, as also explored in Fig. 15, between the input features and corresponding output labels [181]. Supervised learning can be classified into two different types, one is called Regression, while the other is called Classification learning models.

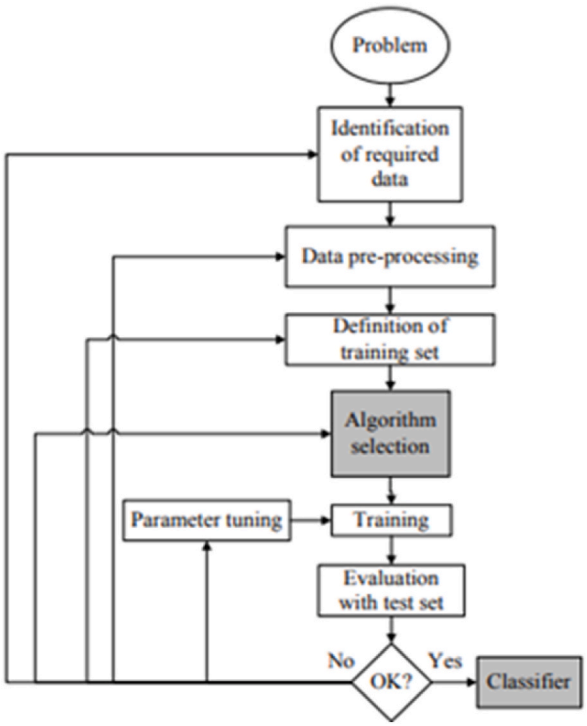

Fig. 14. The Supervised Learning Process [179].

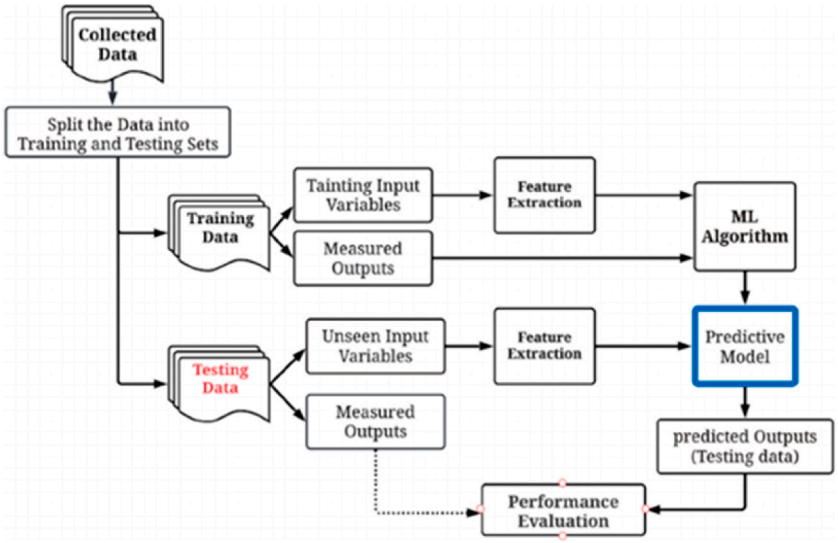

Fig. 15. General model of supervised machine learning [182].

5.3.1. *Regression*

Regression is a supervised learning task that involves the prediction of numerical values, where the algorithm learns the relationship between input features and a target variable, and the goal is to predict or estimate the target variable based on given inputs [183]. Regression models are used in SCC to predict future outcomes for variables, as in Ref. [184], where the corrosion potential and current density are predicted based on input data of electrochemical and mechanical properties of the specimen or material used and the corrosion cell employed.

5.3.2. *Classification*

Classification is a supervised learning task that involves assigning input data into predefined categories or classes, where the algorithm learns a mapping pattern between the input features and the output labels, thus the goal is to correctly classify new instances of data into one of a set of classes based on the given inputs [185]. In SCC, this learning task can be used to identify SCC defects and cracks on structures and parts and classify them correctly as in Ref. [186].

5.4. *Unsupervised learning methods*

Unsupervised learning is a machine learning methodology where the algorithm learns the patterns and relationships in the data

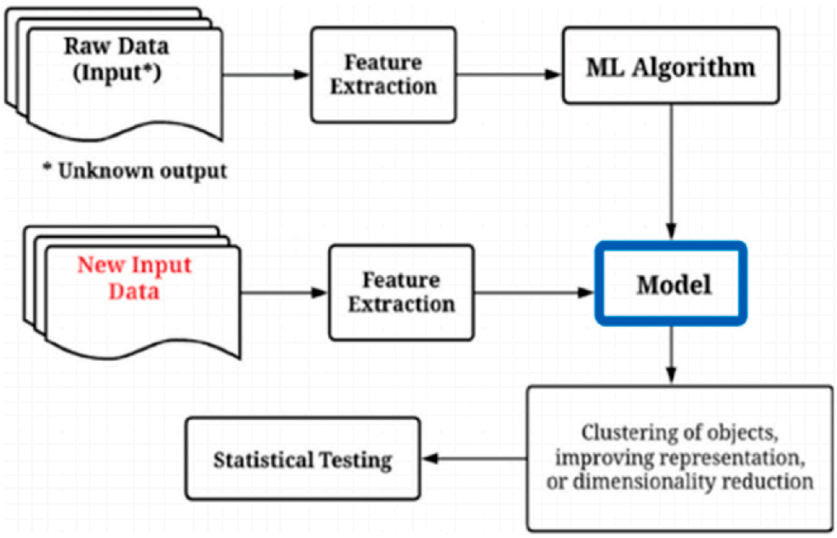

Fig. 16. General model of unsupervised machine learning [182].

without any guidance, training, or labeled examples, which is quite contrary to the supervised learning method, which has target labels or output variables to guide the learning process [187]. Unsupervised learning is used for data analysis, as evident in Fig. 16, in simple terms, it helps researchers eliminate errors and mistakes in the data, helps in processing it, and helps in cleaning it. This can be achieved by utilizing different techniques of unsupervised learning, which include A- Clustering: where similar groups of data are grouped, B- Dimensionality Reduction: where the number of variables or input features are reduced while preserving the important information of the data C- Anomaly Detection: where rare or unusual or deviated data points are identified and D- Association Rule Mining: where interesting associations or relationships between data points are discovered, hence why this method is intensively used for data analysis [188].

5.5. Deep learning methods

Deep learning is a more popular and recent approach to machine learning and artificial intelligence. It focuses on the development and training of deep neural networks, in which multiple layers of interconnected nodes or neurons are used to automatically learn and extract hierarchical representations from the data [189–191]. The human brain inspires deep learning technology and methodology. The general architecture of any deep learning model is an input layer, one or multiple hidden layers, and an output layer, where each layer is made of numerous interconnected nodes or neurons, and each neuron performs mathematical operations on the input data to generate an output. The layers are also densely connected, where each node in one layer is connected to all nodes in the next layer. Additionally, deep learning employs a technique called backpropagation, in which the network iteratively adjusts its internal parameters and values, which are the weights and biases, to minimize the difference between the predictions and true values in the training data [192]. Fig. 17 shows an example for a multi-layer deep learning model, which can be as simple as the inclusion of a couple of layers to give an output (Fig. 17a), or as complex as including multiple multi-node layers to provide accurate predictions and evaluations (Fig. 17b).

There are many methods and types of deep learning with different architectures and for different applications, and usually, these different methods and types are mixed to create a new type for a certain cause, this can be as simple as the reduction of computational power, enhancing the accuracy and efficiency, or other reasons. The following is a sample of the well-known methods and the use of each for the prognosis of SCC in metals and mechanical parts.

5.5.1. Convolutional neural networks (CNNs)

CNNs are a type of deep learning neural network, it is generally used for grid-structured data, which can be images or time-series data, and they have been widely employed in computer vision applications and achieved success in image classification, object detection, and image segmentation applications [194]. It is made of convolutional layers, which perform filtering on the inputs, which is done by taking the dot-product between the filter and a small portion of the input data at a time to capture local patterns and features, and activation functions which are used to introduce element-wise non-linearities to the CNN, and pooling layers which are employed to down-sample the feature maps obtained from the convolutional layers, and fully connected layers which are similar to the layer architecture of a tradition deep learning model. CNNs can be applied in the prognosis of SCC by analyzing image-based or visual data on the material surface or microstructure, where the propagation pattern or initiation of the cracks can be studied and predicted, or ultrasonic testing data can be analyzed to identify and determine the extent of SCC damage on materials [195].

5.5.2. Recurrent neural networks (RNNs)

RNNs are a type of deep neural network designed to process data with temporal dependencies, such as time-series data, where unlike typical CNNs (which are called feedforward) they can process data in a feedback manner, allowing them to persist and flow in a loop [196]. Thus, RNNs are the choice when the data available is sequential with time dependencies. In SCC, this type of neural network (NN) model is best used to predict numerical data based on history, such as the corrosion rate, current density, or corrosion potential, and it can be used with ultrasonic test results to analyze the history of the data and results and predict the crack propagation behavior in the future [197]. Lastly, RNNs can be mixed with CNNs to employ a spatio-temporal model, which can be used to predict the crack propagation behavior and pattern based on an input sequence of images of the crack over time, taking into consideration the crack length and crack propagation rate.

5.5.3. Generative adversarial networks (GANs)

GANs are a class of deep learning NNs, that are used to create synthetic data using two sub-neural networks that work together competitively, the first sub-network is called the generator network, while the second is the discriminator network, and the two networks are trained together to generate realistic data samples and the discriminator tries to distinguish between the real and fake data samples [198]. This model can be used to generate realistic synthetic data for SCC cases to train other artificial intelligence models, such as creating synthetic images or synthetic time-series data.

5.5.4. Long short-term memory (LSTM)

This model is a type of RNN architecture that addresses the vanishing gradient problem in the traditional RNN models and enables the model to capture long-term dependencies in the sequential data, hence this model is crucial in tasks where understanding the context of the data and remembering past information is needed, which is why it is generally employed and successful in time-series cases [199]. This is all achieved by a key feature called the memory cell which allows the model to remember and retain long-term past information in the data. This model can be used in the same manner as RNNs for the prognosis of SCC but with better performance and

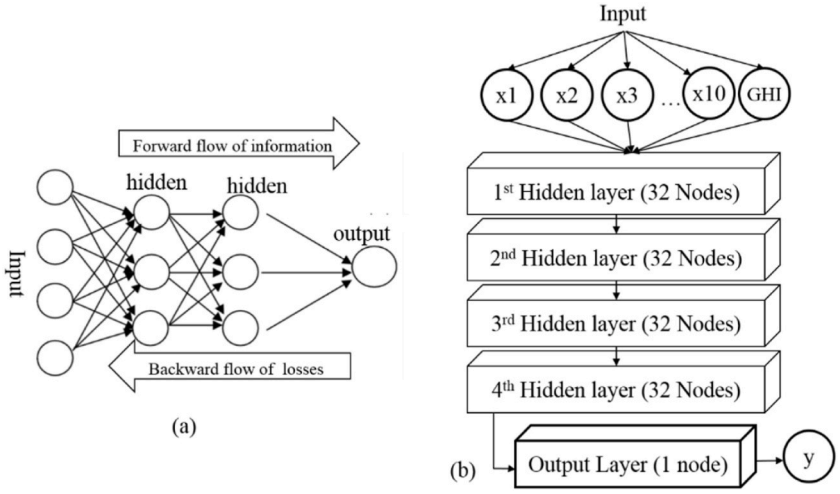

Fig. 17. An Example of a Multi-Layer Deep Learning Model with a Single Output for Quantification Tasks. a) Shows a Simple Model, and b) Shows a Model Proposed by Aslam et al. [193].

higher accuracy due to the long-term memory factor.

Table 3 outlines an array of AI techniques, each tailored to specific applications and materials for SCC prognosis. While these methods offer innovative approaches, the inconsistency in accuracy metrics across the studies calls for a more standardized evaluation process to reliably gauge their effectiveness. However, as for the other comparisons, the works done toward SCC prognosis using AI provide rich data and frameworks to be used for the prediction of different conditions and natures.

6. Conclusions and future directions for SCC prognosis

It is evident from Table 1, we note that non-destructive techniques are viable to detect and predict SCC flaws in materials and parts during and after real-life working conditions, we note that they are mostly used to detect corrosion pits and cracks, which would lead eventually to failure of the parts and materials. However, we see that machine learning and artificial intelligence techniques are becoming increasingly viable and accurate in predicting SCC defects and material failures. We note from Table 3 that classical AI techniques are the most used among the discussed options, with regression, supervised, and unsupervised techniques leading the way in the prognosis process of SCC, so we can conclude that intensive use of deep learning techniques, including the ones with past correlative capabilities (such as LSTM, RNN, and Gated Recurrent Units) would be the systems to take the lead in the future, and this would be a positive due to the lower interference of human workers and inspection personnel, which would protect them from environmental risks, reduce overall time (since the AI model would operate on readily available data), and reduce overall costs (since a computer-based system is what the user or researcher would only need). Hence, we can deduce that intensive studies and the use of AI in predicting, detecting, and studying SCC should be the future direction and point of interest for corrosion and material researchers.

Table 3
Comparison of artificial intelligence techniques.

Ref	Artificial Intelligence Model Used	Application for SCC Prognosis	Environment and Material Case	Accuracy Metrics and/or Results
Xinyu et al. (2020) [200]	Regression Learning	SCC resistance Optimization	Al 7XXX Series Alloy in Simulated Soil Solution	MSE: ±3 Confidence: 99.7 %
Smets & Bogaerts (1992) [201]	Backpropagation CNN	Prediction of SCC Risk in Materials	Austenitic Stainless-Steel Series in a Chloride Solution	The SCC Risk as a Function of the Solution Parameters and Material Treatment (Graphical)
De Masi et al. (2014) [202]	Artificial Neural Network (ANN)	Prediction of Metal Loss and Corrosion Rate Inside a Pipeline	Pipeline Steel Unde H_2S Influence	RMSE: 52 % Correlation Coefficient (R): 0.66 MAE: 31 %
Qian et al. (2022) [203]	CNN & NARX	Prediction of Pitting Corrosion Based on a Phase Field Model	Structural Steel (Building Infrastructure Case)	Within 90 % Confidence Interval
Dourado & Viana (2019) [204]	RNN	Corrosion Fatigue Prognosis for Aircraft	Al 2024-T3 Alloy with Saline Corrosion	Crack Propagation and Damage Assessment and Prognosis
Spanner et al. (2000) [205]	Classification NN	Detection of SCC Flaws Using C-Scans and NN	Austenitic Pipeline Steel	Automation of Ultrasonic Test Data Analysis
Lajevardi et al. (2009) [206]	ANN	Time-to-Failure Prediction	304 Stainless Steel in Chloride Solution	Average Correlation Coefficient: 0.741 Effect of Changing Different Parameters on the Time-to-Failure

Future studies can focus on refining XFEM models to accurately simulate SCC behavior and its interaction with complex microstructures and heterogeneous materials. Moreover, PFM has gained attention for simulating crack dynamics and evolution. Future directions can involve refining PFM techniques to incorporate the influence of environmental factors, such as corrosive species, to capture SCC mechanisms accurately.

To conclude, this research conducted a deep overview of the past, present, and possible future methods in the prognosis and prediction of stress corrosion cracking in materials and parts used in industrial applications. Different methodologies were studied including the non-destructive testing techniques that are currently used, which include ultrasonic testing, eddy current testing, and direct current potential drop testing, which all aim to detect material SCC defects, and a summary table was given to describe research done in this area. Additionally, the electrochemical testing techniques were discussed, including the electrochemical impedance spectroscopy and potentiodynamic polarization techniques, which aim to study the electrochemical properties of the SCC system and how they change with differing cases and conditions. Integrating these simulation techniques with more realistic environmental conditions and material properties will contribute to the development of more accurate predictive models and aid in the design of materials and structures with enhanced resistance to SCC. Nevertheless, the machine learning techniques and algorithms used for the prognosis of SCC have been thoroughly discussed, including the supervised and unsupervised learning algorithms, and the different deep learning algorithms, in addition to a table of summary to describe the different AI algorithms used to predict SCC defects and failures in materials. SCC is a common issue in different industries and to study or simulate it, careful treatments should be taken to consider the accuracy of obtained data, this is true for all of the techniques described in this paper, and the fact remains that with minor inaccuracies, huge variations in the predictions and prognosis can occur, leading to false conclusions and estimation for the SCC failure, which would lead to huge losses to the industries. It is noted that future research is moving in the direction of AI, which would help us conclude that machine learning technology would be the main research focus for different applications and areas of interest, including SCC, in the coming years.

Author contributions

Mohammad Alkhedher: Writing – review & editing, Supervision, Methodology, Funding acquisition. Omer Mughieda: Writing – review & editing, Resources, Conceptualization. Aghyad B. Al Tahhan: Methodology, Conceptualization. Mutasem A. Shehadeh: Writing – review & editing, Supervision, Methodology. Abdel-Hamid I. Mourad: Writing – review & editing, Supervision, Methodology. Abdullah Alsit: Writing – original draft, Methodology, Conceptualization. Hasan Hamdan: Writing – original draft, Methodology, Conceptualization

Funding statement

This research is supported by ASPIRE, the technology program management pillar of Abu Dhabi's Advanced Technology Research Council (ATRC), via the ASPIRE "AARE (ASPIRE Awards for Research Excellence)".

Data availability

No data was used for the research described in the article.

Declaration of competing interest

The authors declare the following financial interests/personal relationships which may be considered as potential competing interests:Mohammad Alkhedher reports financial support was provided by Advanced Technology Research Council.

References

[1] Z. Fan, X. Hu, J. Liu, H. Li, J. Fu, Stress corrosion cracking of L360NS pipeline steel in sulfur environment, Petroleum 3 (2017) 377–383, https://doi.org/10.1016/j.petlm.2017.03.006.
[2] Z. Ren, F. Ernst, Stress–corrosion cracking of AISI 316L stainless steel in seawater environments: effect of surface machining, Metals 10 (2020) 1–17, https://doi.org/10.3390/met10101324.
[3] S. Shipilov, F. King, Pipeline stress corrosion cracking: direction and control, Mater. Perform. 54 (2015) 30–37.
[4] W. Chen, Modeling and prediction of stress corrosion cracking of pipeline steels, in: Trends in Oil and Gas Corrosion Research and Technologies: Production and Transmission, Elsevier Inc., 2017, pp. 707–748, https://doi.org/10.1016/B978-0-08-101105-8.00030-9.
[5] A. Turnbull, Modeling of the chemistry and electrochemistry in cracks—a review, Corrosion 57 (2001) 175–189, https://doi.org/10.5006/1.3290342.
[6] M. Wasim, M.B. Djukic, External corrosion of oil and gas pipelines: a review of failure mechanisms and predictive preventions, J. Nat. Gas Sci. Eng. 100 (2022) 104467, https://doi.org/10.1016/j.jngse.2022.104467.
[7] Z. Lu, Y. Takeda, T. Shoji, Some fundamental aspects of thermally activated processes involved in stress corrosion cracking in high temperature aqueous environments, J. Nucl. Mater. 383 (2008) 92–96, https://doi.org/10.1016/j.jnucmat.2008.08.051.
[8] Z. Zhang, X. Wu, J. Tan, In-situ monitoring of stress corrosion cracking of 304 stainless steel in high-temperature water by analyzing acoustic emission waveform, Corrosion Sci. 146 (2019) 90–98, https://doi.org/10.1016/j.corsci.2018.10.022.
[9] S. Wu, J. Li, J. Guo, G. Shi, Q. Gu, C. Lu, Stress corrosion cracking fracture mechanism of cold-drawn high-carbon cable bolts, Mater. Sci. Eng., A 769 (2020) 138479, https://doi.org/10.1016/j.msea.2019.138479.
[10] D. Féron, C. Guerre, E. Herms, P. Laghoutaris, 9 - stress corrosion cracking of Alloy 600: overviews and experimental techniques, in: D. Féron, R.W. Staehle (Eds.), Stress Corrosion Cracking of Nickel Based Alloys in Water-Cooled Nuclear Reactors, Woodhead Publishing, 2016, pp. 325–353, https://doi.org/10.1016/B978-0-08-100049-6.00009-4.

[11] Y. Cui, C. Li, S. Harjo, C. Zhang, R. Li, W. Zheng, Y. Wang, A Study on the Micromechanical Behavior of Ti-55531 Titanium Alloy with Lamellar Microstructure by In-Situ Neutron Diffraction, 2020. https://scite.ai/reports/10.1051/matecconf/202032111013.

[12] S. Wang, D.K. Xu, E.-H. Han, C. Dong, Stress corrosion cracking susceptibility of a high strength Mg-7%Gd-5%Y-1%Nd-0.5%Zr alloy, J. Magnesium Alloys 2 (2014) 335–341, https://doi.org/10.1016/j.jma.2014.11.004.

[13] K. Thakur, A. Nagpal, Mayank, V. Mahajan, I.A. Bhat, Biomaterials in implantology: a review, Ip Annals of Prosthodontics and Restorative Dentistry 4 (2020) 111–113, https://doi.org/10.18231/2581-480x.2018.0029.

[14] N.J.H. Holroyd, G.M. Scamans, Stress corrosion cracking in Al-Zn-Mg-Cu aluminum alloys in saline environments, Metall. Mater. Trans. 44 (2013) 1230–1253, https://doi.org/10.1007/s11661-012-1528-3.

[15] F. Yang, H. Xue, L. Zhao, X. Fang, Effects of welded mechanical heterogeneity on interface crack propagation in dissimilar weld joints, Adv. Mater. Sci. Eng. 2019 (2019) 6593982, https://doi.org/10.1155/2019/6593982.

[16] T. Lucas, A. Forsström, T. Saukkonen, R. Ballinger, H. Hänninen, Effects of thermal aging on material properties, stress corrosion cracking, and fracture toughness of AISI 316L weld metal, Metall. Mater. Trans. 47 (2016) 3956–3970, https://doi.org/10.1007/s11661-016-3584-6.

[17] A.K. Mukhopadhyay, Microstructure and Properties of High Strength Aluminium Alloys for Structural Applications, vol. 62, Transactions of the Indian Institute of Metals, 2009, pp. 113–122, https://doi.org/10.1007/s12666-009-0015-z.

[18] W. Hao, Z. Liu, W. Wu, X. Li, C. Du, D. Zhang, Electrochemical characterization and stress corrosion cracking of E690 high strength steel in wet-dry cyclic marine environments, Mater. Sci. Eng., A 710 (2018) 318–328, https://doi.org/10.1016/j.msea.2017.10.042.

[19] B. Dubuc, A. Ebrahimkhanlou, S. Salamone, Stress monitoring of prestressing strands in corrosive environments using modulated higher-order guided ultrasonic waves, Struct. Health Monit. 19 (2019) 202–214, https://doi.org/10.1177/1475921719842385.

[20] I.B. Obot, I.B. Onyeachu, S.A. Umoren, M.A. Quraishi, A.A. Sorour, T. Chen, N. Aljeaban, Q. Wang, High temperature sweet corrosion and inhibition in the oil and gas industry: progress, challenges and future perspectives, J. Pet. Sci. Eng. 185 (2020) 106469, https://doi.org/10.1016/j.petrol.2019.106469.

[21] D. Du, K. Chen, H. Lu, L. Zhang, X. Shi, X. Xu, P.L. Andresen, Effects of chloride and oxygen on stress corrosion cracking of cold worked 316/316L austenitic stainless steel in high temperature water, Corrosion Sci. 110 (2016) 134–142, https://doi.org/10.1016/j.corsci.2016.04.035.

[22] K. Tohgo, H. Suzuki, Y. Shimamura, G. Nakayama, T. Hirano, Monte Carlo simulation of stress corrosion cracking on a smooth surface of sensitized stainless steel type 304, Corrosion Sci. 51 (2009) 2208–2217, https://doi.org/10.1016/j.corsci.2009.06.013.

[23] V. Giorgetti, E.A. Santos, J.B. Marcomini, V.L. Sordi, Stress corrosion cracking and fatigue crack growth of an API 5L X70 welded joint in an ethanol environment, Int. J. Pres. Ves. Pip. 169 (2019) 223–229, https://doi.org/10.1016/j.ijpvp.2019.01.006.

[24] D. Han, H. Fan, C. Yan, T. Wang, Y. Yang, S. Ali, G. Wang, Heat conduction and cracking of functionally graded materials using an FDEM-based thermo-mechanical coupling model, Appl. Sci. 12 (2022), https://doi.org/10.3390/app122312279.

[25] P.B. Srinivasan, S. Riekehr, C. Blawert, W. Dietzel, M. Koçak, Mechanical properties and stress corrosion cracking behaviour of AZ31 magnesium alloy laser weldments, Trans. Nonferrous Metals Soc. China 21 (2011) 1–8, https://doi.org/10.1016/S1003-6326(11)60670-5.

[26] S. Moore, R. Burrows, L. Picco, T.L. Martin, S.J. Greenwell, T.B. Scott, O.D. Payton, A study of dynamic nanoscale corrosion initiation events using HS-AFM, Faraday Discuss 210 (2018) 409–428, https://doi.org/10.1039/C8FD00017D.

[27] S. Rossi, F. Russo, A.M. Lemmi, M. Benedetti, V. Fontanari, Fatigue corrosion behavior of friction welded dissimilar joints in different testing conditions, Metals 10 (2020) 1018, https://doi.org/10.3390/met10081018.

[28] L. Zhao, Z. Shi, Z. Wang, F. Yang, An investigation of a new parameter based on the plastic strain gradient to characterize composite constraint around the crack front at a low temperature, Materials 15 (2022) 881, https://doi.org/10.3390/ma15030881.

[29] Z. Su, J. Xin, Q. Zhang, J. Chen, Y. Guo, Transient force-magnetic coupling simulation research on pipeline stress concentration, J Phys Conf Ser 2383 (2022) 12151, https://doi.org/10.1088/1742-6596/2383/1/012151.

[30] Z. Zhang, Y. Yu, J. Zhang, X.-J. Wang, Corrosion behavior of keyhole-free friction stir spot welded joints of dissimilar 6082 aluminum alloy and DP600 galvanized steel in 3.5% NaCl solution, Metals 7 (2017) 338, https://doi.org/10.3390/met7090338.

[31] D. Dwivedi, K. Lepkova, T. Becker, Carbon steel corrosion: a review of key surface properties and characterization methods, RSC Adv. 7 (2017) 4580–4610, https://doi.org/10.1039/c6ra25094g.

[32] G. Vizentin, G. Vukelić, D.-S. Cho, N. Recho, J. Orović, Marine propulsion system failures—a review, J. Mar. Sci. Eng. 8 (2020) 662–676, https://doi.org/10.3390/jmse8090662.

[33] S. Yurtdaş, U. İnce, B. Tanrıkulu, C. Kılıçaslan, M.B. Toparli, Corrosion effects on fatigue behavior of Zn-Cr+3 and Zn flake coated M8 DIN 933 bolts, Sakarya University Journal of Science 25 (2021) 867–874, https://doi.org/10.16984/saufenbilder.796745.

[34] A.K. Singh, A.S. Rao, Blade lock ring of 4th stage compressor rotor: failure investigation, International Journal of Engineering Materials and Manufacture 4 (2019) 85–95, https://doi.org/10.26776/ijemm.04.03.2019.01.

[35] M. Lara-Banda, C. Gaona-Tiburcio, P. del Carmen Zambrano-Robledo, M. Delgado-E, J. Cabral-Miramontes, D. Nieves-Mendoza, E. Maldonado-Bandala, F. Estupiñan-López, J.G. Chacón-Nava, F. Almeraya-Calderón, Alternative to nitric acid passivation of 15-5 and 17-4PH stainless steel using electrochemical techniques, Materials 13 (2020) 2836, https://doi.org/10.3390/ma13122836.

[36] J. Sun, J. Ding, S. Chen, J. Li, Numerical Simulation of Centrifugal Compressor Impeller Flow Field Based on ANSYS Workbench, 2015, https://doi.org/10.2991/icadme-15.2015.90.

[37] T. Fujii, M.S.B.M. Azmi, K. Tohgo, Y. Shimamura, Influence of strain gradient on fatigue life of carbon steel for pressure vessels in low-cycle and high-cycle fatigue regimes, Materials 15 (2022) 445, https://doi.org/10.3390/ma15020445.

[38] P. Peterka, J. Krešák, The causes of the damage to the bearing rope – the FAILUREANALYSIS, Advances in Science and Technology – Research Journal 12 (2018) 231–236, https://doi.org/10.12913/22998624/92341.

[39] W. Li, M. Wu, T. Shi, P. Yang, Z. Pan, W. Liu, J. Liu, X. Yang, Experimental investigation of the relationship between surface crack of concrete cover and corrosion degree of steel bar using fractal theory, Fractal and Fractional 6 (2022) 325, https://doi.org/10.3390/fractalfract6060325.

[40] G.P. Pellizzer, E.D. Leonel, Probabilistic corrosion time initiation modelling in reinforced concrete structures using the BEM, Revista Ibracon De Estruturas E Materiais 13 (2020), https://doi.org/10.1590/s1983-41952020000400009.

[41] C.C. Silva, J.T. de Assis, S. Philippov, J.P. Farias, Residual stress, microstructure and hardness of thin-walled low-carbon steel pipes welded manually, Mater. Res. 19 (2016) 1215–1225, https://doi.org/10.1590/1980-5373-mr-2016-0217.

[42] T.L. Mader, Environmental factors influencing heat stress in feedlot cattle, J. Anim. Sci. 84 (2006) 712–719, https://doi.org/10.2527/2006.843712X.

[43] S. Wu, H. Chen, H.L. Ramandi, P.C. Hagan, A. Crosky, S. Saydam, Effects of environmental factors on stress corrosion cracking of cold-drawn high-carbon steel wires, Corrosion Sci. 132 (2018) 234–243, https://doi.org/10.1016/j.corsci.2017.12.014.

[44] M.E. McMahon, Z.D. Harris, J.R. Scully, J.T. Burns, The effect of electrode potential on stress corrosion cracking in highly sensitized Al–Mg alloys, Mater. Sci. Eng., A 767 (2019) 138399, https://doi.org/10.1016/j.msea.2019.138399.

[45] B.T. Lu, Z.K. Chen, J.L. Luo, B.M. Patchett, Z.H. Xu, Pitting and stress corrosion cracking behavior in welded austenitic stainless steel, Electrochim. Acta 50 (2005) 1391–1403, https://doi.org/10.1016/j.electacta.2004.08.036.

[46] Y.F. Cheng, Fundamentals of hydrogen evolution reaction and its implications on near-neutral pH stress corrosion cracking of pipelines, Electrochim. Acta 52 (2007) 2661–2667, https://doi.org/10.1016/j.electacta.2006.09.024.

[47] Z. Lu, T. Shoji, Y. Takeda, Y. Ito, A. Kai, N. Tsuchiya, Effects of loading mode and water chemistry on stress corrosion crack growth behavior of 316L HAZ and weld metal materials in high temperature pure water, Corrosion Sci. 50 (2008) 625–638, https://doi.org/10.1016/j.corsci.2007.08.021.

[48] J. Sanchez, C. Andrade, J. Fullea, Reasons for crack arrest in stress corrosion cracking tests—crack propagation rate in high-strength steels, Corrosion 65 (2009) 368–375, https://doi.org/10.5006/1.3319142.

[49] X. Lou, D. Yang, P.M. Singh, Film breakdown and anodic dissolution during stress corrosion cracking of carbon steel in bioethanol, J. Electrochem. Soc. 157 (2010) C86, https://doi.org/10.1149/1.3269927.

[50] K. Hirano, S. Ishizaki, H. Kobayashi, H. Nakazawa, Determination of threshold stress corrosion cracking characteristics using rising load KIscc testing based on ultrasonic method, J. Test. Eval. 13 (1985) 162–168, https://doi.org/10.1520/JTE10775J.

[51] F. Morlock, L.J. Jacobs, J.-Y. Kim, P.M. Singh, J.J. Wall, Nonlinear Ultrasonic Assessment of Stress Corrosion Cracking Damage in Sensitized 304 Stainless Steel, American Institute of PhysicsAIP, 2015, https://doi.org/10.1063/1.4914785.

[52] F. Hernandez-Valle, A.R. Clough, R.S. Edwards, Stress corrosion cracking detection using non-contact ultrasonic techniques, Corrosion Sci. 78 (2014) 335–342, https://doi.org/10.1016/J.CORSCI.2013.10.018.

[53] M.K. Chang, H.S. Sun, J.C. Ciou, Applying ultrasonic testing to detect hole defect near the surface, Adv. Mater. Res. (2011) 2054–2057, https://doi.org/10.4028/WWW.SCIENTIFIC.NET/AMR.194-196.2054.

[54] W.M. Wright, D.A. Hutchins, Air-coupled ultrasonic testing of metals using broadband pulses in through-transmission, Ultrasonics 37 (1999) 19–22, https://doi.org/10.1016/S0041-624X(98)00034-1.

[55] V. V Murashov, S.I. Yakovleva, Research and Improvement of Noncontacting Technique of the Ultrasonic through Transmission Method of Non-destructive Testing, vol. 258, Izdatel'skii Dom Spektr, LLC, 2019, pp. 16–22, https://doi.org/10.14489/td.2019.12.pp.016-022.

[56] M.R. Mitchell, R.E. Link, C. Stergiopoulou, R.H. McCuen, M.S. Aggour, Ultrasonic testing of concrete structures using indirect transmission, J. Test. Eval. 36 (2008) 2, https://doi.org/10.1520/JTE101158.

[57] G. Waag, L. Hoff, P. Norli, Air-coupled ultrasonic through-transmission thickness measurements of steel plates, Ultrasonics 56 (2015) 332–339, https://doi.org/10.1016/J.ULTRAS.2014.08.021.

[58] H.W." ustenberg, A. Erhard, H.-J. Montag, G. Schenk, Measurement of Crack Depth with Ultrasonic Methods — through Transmission- and Reflection Modes, New Procedures in Nondestructive Testing, 1983, pp. 213–228, https://doi.org/10.1007/978-3-662-02363-1_20.

[59] B. Mojškerc, T. Kek, J. Grum, Pulse-echo ultrasonic testing of adhesively bonded joints in glass façades, Strojniski Vestnik-Journal of Mechanical Engineering 62 (2016) 147–153, https://doi.org/10.5545/SV-JME.2015.2988.

[60] S. Kumaran, B.S. Rani, Application of synthetic aperture focusing technique for estimation of width using pulse echo ultrasonic testing, Indian J. Sci. Technol. 7 (2014) 396–400, https://doi.org/10.17485/IJST/2014/V7I4.7.

[61] T.G. Alvarez-Arenas, J. Camacho, Air-coupled and resonant pulse-echo ultrasonic technique, Sensors 19 (2019) 10, https://doi.org/10.3390/S19102221.

[62] H.G. Tattersall, The ultrasonic pulse-echo technique as applied to adhesion testing, J. Phys. D Appl. Phys. 6 (1973) 819–832, https://doi.org/10.1088/0022-3727/6/7/305.

[63] Y.H. Kim, S.-J. Song, S. Lee, J.B. Lee, S.-S. Hong, H.S. Eom, A study of the couplant effects on contact ultrasonic testing, Journal of the Korean Society for Nondestructive Testing 22 (2002) 621–626.

[64] M. Youssef, N. Gobran, Modified treatment of ultrasonic pulse-echo immersion technique, Ultrasonics 39 (2002) 473–477, https://doi.org/10.1016/S0041-624X(01)00085-3.

[65] C.J. Lissenden, I. Jovanovic, A.T. Motta, X. Xiao, L. Berre, D.C.S.S. Fobar, Remote detection of stress corrosion cracking: surface composition and crack detection, AIP Conf. Proc. 1949 (2018) 1, https://doi.org/10.1063/1.5031582.

[66] D. Mukherjee, S. Sarkar, N. Sen, K.K. Singh, S. Saha, S. Mehetre, A. Mayya, K.T. Shenoy, Non-invasive monitoring of segregated phases in a biogas plant: an ultrasonic approach, Results in Engineering 14 (2022) 100477, https://doi.org/10.1016/j.rineng.2022.100477.

[67] S. Petit, M. Duquennoy, M. Ouaftouh, F. Deneuville, M. Ourak, S. Desvaux, Non-destructive testing of ceramic balls using high frequency ultrasonic resonance spectroscopy, Ultrasonics 43 (2005) 802–810, https://doi.org/10.1016/J.ULTRAS.2005.06.003.

[68] T.M. Yoshandi, H.E. Hamdani, Annisa, material analysis of lead aprons using radiography non-destructive testing, Journal Renewable Energy & Mechanics 4 (2021) 56–62, https://doi.org/10.25299/REM.2021.VOL4.NO02.7480.

[69] C. Jung, Y. Kang, H. Song, M.G. Lee, Y. Jeon, Ultrasonic fatigue analysis of 3D-printed carbon fiber reinforced plastic, Heliyon 8 (11) (2022) e11671, https://doi.org/10.1016/j.heliyon.2022.e11671.

[70] A.B. Lopez, R. Bacelar, I. Pires, T.G. Santos, J.P. Sousa, L. Quintino, Non-destructive testing application of radiography and ultrasound for wire and arc additive manufacturing, Addit. Manuf. 21 (2018) 298–306, https://doi.org/10.1016/J.ADDMA.2018.03.020.

[71] R. Arbol, P. M, P.G. Garcia, C.D. Gonzalez, A. OrioAlonso, Non-destructive testing of industrial equipment using muon radiography, Philosophical Transactions of the Royal Society A 377 (2019) 2137, https://doi.org/10.1098/RSTA.2018.0054.

[72] S.M. Kang, C.-H. Shin, V. Ha, P. N, C.I. Chol, J.K. Kim, Y.K. Kim, Comparison to images from a computed radiography system for non-destructive testing using selenium-75, iridium-192, and X-rays, J. Kor. Phys. Soc. 59 (2011) 717–720, https://doi.org/10.3938/jkps.59.717.

[73] M.R. Sameye, A.M. Bahalkeh, A. Izadi, A. Jafaryan, Comparison of Digital Radiography, Conventional Film and Self-Developing Film for Working Length Determination, vol. 13, 2018, pp. 381–384, https://doi.org/10.22037/IEJ.V13I3.19355.

[74] A. Sophian, G. Tian, M. Fan, Pulsed eddy current non-destructive testing and evaluation: a review, Chin. J. Mech. Eng. 30 (2017) 500–514, https://doi.org/10.1007/S10033-017-0122-4.

[75] B. Helifa, A. Oulhadj, A. Benbelghit, I.K. Lefkaier, F. Boubenider, D. Boutassouna, Detection and measurement of surface cracks in ferromagnetic materials using eddy current testing, NDT E Int. 39 (2006) 384–390, https://doi.org/10.1016/J.NDTEINT.2005.11.004.

[76] R. Palanisamy, Electromagnetic field calculations for the low frequency eddy current testing of tubular products, IEEE Trans. Magn. 23 (1987) 2663–2665, https://doi.org/10.1109/TMAG.1987.1065698.

[77] N. Yusa, L. Janousek, M. Rebican, Z. Chen, K. Miya, N. Chigusa, H. Ito, Detection of embedded fatigue cracks in Inconel weld overlay and the evaluation of the minimum thickness of the weld overlay using eddy current testing, Nucl. Eng. Des. 236 (2006) 1852–1859, https://doi.org/10.1016/J.NUCENGDES.2006.02.011.

[78] Y. Zhao, P. Qi, Z. Xie, P. Bai, H.-E. Chen, S. Xie, Z. Chen, A new array eddy current testing probe for inspection of small-diameter tubes in Tokamak fusion devices, Fusion Eng. Des. 157 (2020).

[79] N. Kobayashi, S. Ueno, S. Nagai, M. Ochiai, N. Jimbo, Remote field eddy current testing for steam generator inspection of fast reactor, Nucl. Eng. Des. 241 (2011) 4643–4648, https://doi.org/10.1016/J.NUCENGDES.2011.03.054.

[80] S. Sudirman, F. Natalia, A. Sophian, A. Ashraf, Pulsed Eddy Current signal processing using wavelet scattering and Gaussian process regression for fast and accurate ferromagnetic material thickness measurement, Alex. Eng. J. 61 (12) (2022) 11239–11250, https://doi.org/10.1016/j.aej.2022.04.028.

[81] K. V Minnebruggen, S. Hertelé, M. Verstraete, W. De Waele, Crack growth characterization in single-edge notched tension testing by means of direct current potential drop measurement, Int. J. Pres. Ves. Pip. 156 (2017) 68–78, https://doi.org/10.1016/J.IJPVP.2017.06.009.

[82] J. Zhang, S. Xie, X. Wang, Y. Li, Z. Chen, Quantitative non-destructive testing of metallic foam based on direct current potential drop method, IEEE Trans. Magn. 48 (2012) 375–378, https://doi.org/10.1109/TMAG.2011.2172679.

[83] S. Shrestha, M. Kannan, G.N. Morscher, M.J. Presby, S.M. Razavi, In-situ fatigue life analysis by modal acoustic emission, direct current potential drop and digital image correlation for steel, Int. J. Fatig. 142 (2021) 4, https://doi.org/10.1016/J.IJFATIGUE.2020.105924.

[84] S. Na, D.H. Yoon, J.-H. Kim, H.-K. Kim, D. Kim, An evaluation of the fatigue crack propagation rate for powder metallurgical nickel-based superalloys using the DCPD method at elevated temperatures, Int. J. Fatig. 101 (2017) 27–35, https://doi.org/10.1016/J.IJFATIGUE.2017.04.003.

[85] W. Cai, S. Xie, C. Jomdecha, X. Wang, C. Pei, N. Li Y. Yusa, Assessment of local conductivity distribution in stress corrosion crack region using direct current potential drop method, Corrosion Sci. 123 (2017) 197–208, https://doi.org/10.1016/j.corsci.2017.01.019.

[86] W. Cai, C. Jomdecha, Y. Zhao, L. Wang, S. Xie, Z. Chen, Quantitative evaluation of electrical conductivity inside stress corrosion crack with electromagnetic NDE methods, Phil. Trans. Math. Phys. Eng. Sci. 378 (2020) 20190589, https://doi.org/10.1098/rsta.2019.0589.

[87] N. Ooka, R. Nishi, Y. Narukawa, M. Takita, K. Yokota, Application of Digital Radiographic Testing techniques–Experiments on Detection of Fatigue Crack and Stress Corrosion Cracking. 15th Asia Pacific Conference for Non-destructive Testing (APCNDT2017), 2017. Singapore.

[88] J. Wang, H. Su, K. Chen, D. Du, L. Zhang, Z. Shen, Effect of δ-ferrite on the stress corrosion cracking behavior of 321 stainless steel, Corrosion Sci. 158 (2019) 9, https://doi.org/10.1016/j.corsci.2019.07.005.

[89] N. Yusa, S. Perrin, K. Mizuno, Z. Chen, K. Miya, Eddy current inspection of closed fatigue and stress corrosion cracks, Meas. Sci. Technol. 18 (2007) 3403, https://doi.org/10.1088/0957-0233/18/11/021.

[90] D. Turcio-Ortega, D. Fan, P.G. Tratnyek, E.-J. Kim, Y.-S. Chang, Reactivity of Fe/FeS nanoparticles: electrolyte composition effects on corrosion electrochemistry, Environ. Sci. Technol. 46 (2012) 12484–12492, https://doi.org/10.1021/ES303422W.

[91] S. Wang, J. Zhang, O. Gharbi, V. Vivier, M. Gao, M.E. Orazem, Electrochemical impedance spectroscopy, Nature Reviews Methods Primers 1 (2021) 1, https://doi.org/10.1038/s43586-021-00039-w.

[92] J.H. Jang, J.-Y. Yoo, Equivalent circuit evaluation method of lithium polymer battery using bode plot and numerical analysis, IEEE Trans. Energy Convers. 26 (2011) 290–298, https://doi.org/10.1109/TEC.2010.2089796.

[93] G. Walter, A review of impedance plot methods used for corrosion performance analysis of painted metals, Corrosion Sci. 26 (1986) 681–703, https://doi.org/10.1016/0010-938X(86)90033-8.

[94] Y. Jin-Jie, X. Wei, Equivalent circuits fitting of electrochemical impedance spectroscopy for corrosion of reinforcing steel in concrete, Corrosion Sci. Protect. Technol. 23 (2011) 387–392.

[95] R. Ramesh, D.D. Ebenezer, Equivalent circuit for broadband underwater transducers, IEEE Trans. Ultrason. Ferroelectrics Freq. Control 55 (2008) 2079, https://doi.org/10.1109/TUFFC.899. –2083.

[96] H.R. Bilger, D.H. Lee, M.A. Nicolet, E.R. McCarter, Noise and equivalent circuit of double injection, J. Appl. Phys. 39 (1968) 5913–5918, https://doi.org/10.1063/1.1656089.

[97] M. Sindhuja, N.S. Kumar, V. Sudha, S. Harinipriya, Equivalent circuit modeling of microbial fuel cells using impedance spectroscopy, J. Energy Storage 7 (2016) 136–146, https://doi.org/10.1016/J.EST.2016.06.005.

[98] A. Oskuie, T. Shahrabi, A. Shahriari, E. Saebnoori, Electrochemical impedance spectroscopy analysis of X70 pipeline steel stress corrosion cracking in high pH carbonate solution, Corrosion Sci. 61 (2012) 111–122, https://doi.org/10.1016/j.corsci.2012.04.024.

[99] C. Zheng, G. Yi, Investigating the influence of hydrogen on stress corrosion cracking of 2205 duplex stainless steel in sulfuric acid by electrochemical impedance spectroscopy, Corrosion Rev. 35 (2017) 23–33, 10.1515/corrrev-2016-0060.

[100] F. King, Y. Cheng, L. Gray, B. Drader, R. Sutherby, Field Assessment of FBE-Coated Pipelines and the Implications for Stress Corrosion Cracking, 4th International Pipeline Conference, Calgary, Alberta, 2002.

[101] P. Liang, Y. Guo, H. Qin, Y. Shi, F. Li, L. Jin, Z. Fang, Effects of pH on the electrochemical behavior and stress corrosion cracking of X80 pipeline steel in simulated alkaline soil solution, Int. J. Electrochem. Sci. 14 (2019) 6247–6256, https://doi.org/10.20964/2019.07.09.

[102] S.M. Alavi, A. Mahdi, S.J. Payne, D.A. Howey, Identifiability of generalized Randles circuit models, IEEE Trans. Control Syst. Technol. 25 (2017) 2112–2120, https://doi.org/10.1109/TCST.2016.2635582.

[103] S. Skale, V. Dole cek, M. Slemnik, Substitution of the constant phase element by Warburg impedance for protective coatings, Corrosion Sci. 49 (2007) 1045–1055, https://doi.org/10.1016/J.CORSCI.2006.06.027.

[104] A. Saadi, Y.S.C. Y, B.P.P. Jang C, Passivity breakdown of 316L stainless steel during potentiodynamic polarization in NaCl solution, Corrosion Sci. 111 (2016) 720–727, https://doi.org/10.1016/J.CORSCI.2016.06.011.

[105] M. Curioni, The behaviour of magnesium during free corrosion and potentiodynamic polarization investigated by real-time hydrogen measurement and optical imaging, Electrochim. Acta 120 (2014) 284–292, https://doi.org/10.1016/J.ELECTACTA.2013.12.109.

[106] X. Zhang, Z. Jiang, Z. Yao, Y. Song, Z. Wu, Effects of scan rate on the potentiodynamic polarization curve obtained to determine the Tafel slopes and corrosion current density, Corrosion Sci. 51 (2009) 581–587, https://doi.org/10.1016/J.CORSCI.2008.12.005.

[107] A. Asserghine, M. Medvidović-Kosanović, L. Nagy, R.M. Souto, G. Nagy, A study of the electrochemical reactivity of titanium under cathodic polarization by means of combined feedback and redox competition modes of scanning electrochemical microscopy, Sensor. Actuator. B Chem. 320 (2020) 12833, https://doi.org/10.1016/J.SNB.2020.128339.

[108] A. Asserghine, M. Medvidović-Kosanović, A. Stanković, L. Nagy, R.M. Souto, G. Nagy, A scanning electrochemical microscopy characterization of the localized corrosion reactions occurring on nitinol in saline solution after anodic polarization, Sensor. Actuator. B Chem. 321 (2020) 128610, https://doi.org/10.1016/J.SNB.2020.128610.

[109] A.-R. El-Sayed, H.S. Mohran, H.M. Abd El-Lateef, Corrosion study of zinc, nickel, and zinc-nickel alloys in alkaline solutions by Tafel plot and impedance techniques, Metall. Mater. Trans. 43 (2012) 619–632, https://doi.org/10.1007/s11661-011-0908-4.

[110] A. Yonezu, R. Kusano, X. Chen, On the mechanism of intergranular stress corrosion cracking of sensitized stainless steel in tetrathionate solution, J. Mater. Sci. 48 (2013) 2447–2453, https://doi.org/10.1007/s10853-012-7032-8.

[111] M. Qin, J. Li, S. Chen, Y. Qu, Experimental study on stress corrosion crack propagation rate of FV520B in carbon dioxide and hydrogen sulfide solution, Results Phys. 6 (2016) 365–372, https://doi.org/10.1016/j.rinp.2016.06.012.

[112] H. Ge, J.-L. Le, S.C. Mantell, Numerical modeling of stress corrosion cracking of polymers, Eng. Fract. Mech. 160 (2016) 199–212, https://doi.org/10.1016/j.engfracmech.2016.04.004.

[113] C. Xu, C. Lin, Y. Kang, L. You, An experimental study on porosity and permeability stress-sensitive behavior of sandstone under hydrostatic compression: characteristics, mechanisms and controlling factors, Rock Mech. Rock Eng. 51 (2018) 2321–2338, https://doi.org/10.1007/s00603-018-1481-6.

[114] J. Shi, B. Fekete, J. Wang, D.D. Macdonald, Customization of the coupled environment fracture model for predicting stress corrosion cracking in Alloy 600 in PWR environment, Corrosion Sci. 139 (2018) 58–67, https://doi.org/10.1016/j.corsci.2018.04.039.

[115] S.P. Lynch, 1 - mechanistic and fractographic aspects of stress-corrosion cracking (SCC), in: V.S. Raja, T. Shoji (Eds.), Stress Corrosion Cracking, Woodhead Publishing, 2011, pp. 3–89, https://doi.org/10.1533/9780857093769.1.3.

[116] A. Alsit, M. Alkhedher, H. Hamdan, Crack propagation in pipelines under extreme conditions of near-neutral PH SCC, Comput. Mater. Continua (CMC) 73 (2022) 5315–5329.

[117] S.-J. Lee, Y.-S. Chang, Evaluation of primary water stress corrosion cracking growth rates by using the extended finite element method, Nucl. Eng. Technol. 47 (2015) 895–906, https://doi.org/10.1016/j.net.2015.08.003.

[118] T. Misawa, The corrosion fatigue and stress corrosion cracking of α-brass in ammoniacal solutions, Corrosion Sci. 18 (1978) 199–216, https://doi.org/10.1016/S0010-938X(78)80018-3.

[119] D.D. Macdonald, Passivity–the key to our metals-based civilization 71 (1999) 951–978, 10.1351/pac199971060951.

[120] A.P. Jivkov, Strain-induced passivity breakdown in corrosion crack initiation, Theor. Appl. Fract. Mech. 42 (2004) 43–52, https://doi.org/10.1016/j.tafmec.2004.06.004.

[121] R.N. Parkins, Current topics in corrosion: factors influencing stress corrosion crack growth kinetics, Corrosion 43 (1987) 130–139, https://doi.org/10.5006/1.3583125.

[122] F.P. Ford, 3 mechanisms of environmentally-assisted cracking, Int. J. Pres. Ves. Pip. 40 (1989) 343–362, https://doi.org/10.1016/0308-0161(89)90097-5.

[123] S. Gavrilov, M. Vankeerberghen, G. Nelissen, J. Deconinck, Finite element calculation of crack propagation in type 304 stainless steel in diluted sulphuric acid solutions, Corrosion Sci. 49 (2007) 980–999, https://doi.org/10.1016/j.corsci.2006.06.025.

[124] J.R. Galvele, Surface mobility mechanism of stress-corrosion cracking, Corrosion Sci. 35 (1993) 419–434, https://doi.org/10.1016/0010-938X(93)90175-G.

[125] K. Sieradzki, F.J. Friedersdorf, Notes on the surface mobility mechanism of stress-corrosion cracking, Corrosion Sci. 36 (1994) 669–675, https://doi.org/10.1016/0010-938X(94)90072-8.

[126] J. Sanchez, J. Fullea, C. Andrade, Fracto-surface mobility mechanism in high-strength steel wires, Eng. Fract. Mech. 186 (2017) 410–422, https://doi.org/10.1016/j.engfracmech.2017.11.003.

[127] G.E. Rhead, Surface defects, Surf. Sci. 68 (1977) 20–38, https://doi.org/10.1016/0039-6028(77)90186-8.

[128] JoséR. Galvele, A stress corrosion cracking mechanism based on surface mobility, Corrosion Sci. 27 (1987) 1–33, https://doi.org/10.1016/0010-938X(87)90117-X.

[129] Y. Wada, A. Watanabe, M. Tachibana, N. Uetake, S. Uchida, K. Ishigure, Effects of hydrogen peroxide on intergranular stress corrosion cracking of stainless steel in high temperature water, (III), J. Nucl. Sci. Technol. 37 (2000) 901–912, https://doi.org/10.1080/18811248.2000.9714971.
[130] W. Wu, Z. Liu, X. Li, C. Du, Z. Cui, Influence of different heat-affected zone microstructures on the stress corrosion behavior and mechanism of high-strength low-alloy steel in a sulfurated marine atmosphere, Mater. Sci. Eng., A 759 (2019) 124–141, https://doi.org/10.1016/j.msea.2019.05.024.
[131] D. Kovalov, B. Fekete, G.R. Engelhardt, D.D. Macdonald, Prediction of corrosion fatigue crack growth rate in alloys. Part II: effect of electrochemical potential, NaCl concentration, and temperature on crack propagation in AA2024-T351, Corrosion Sci. 152 (2019) 130–139, https://doi.org/10.1016/j.corsci.2019.03.005.
[132] M. Liu, J. Guo, C.-Y. Hui, A. Zehnder, Crack tip stress based kinetic fracture model of a PVA dual-crosslink hydrogel, Extreme Mech Lett 29 (2019) 100457, https://doi.org/10.1016/j.eml.2019.100457.
[133] M.M. Hall, Effect of variable stress intensity factor on hydrogen environment assisted cracking, Metall. Mater. Trans. 42 (2011) 304–318, https://doi.org/10.1007/s11661-010-0226-2.
[134] P.M. Scott, M. Le Calver, Some Possible Mechanisms of Intergranular Stress Corrosion Cracking of Alloy 600 in PWR Primary Water, Minerals, Metals Ampersand Materials Society, 1993. United States, http://inis.iaea.org/search/search.aspx?orig_q=RN:25067219.
[135] K. Sieradzki, R.C. Newman, Stress-corrosion cracking, J. Phys. Chem. Solid. 48 (1987) 1101–1113, https://doi.org/10.1016/0022-3697(87)90120-X.
[136] C. Zhang, F. Chen, M.H. Gray, R. Tirawat, R.E. Larsen, An elasto-plastic solution for channel cracking of brittle coating on polymer substrate, Int. J. Solid Struct. 120 (2017) 125–136, https://doi.org/10.1016/j.ijsolstr.2017.04.033.
[137] H.-J. Christ, K. Wackerman, U. Krupp, On the mechanism of dynamic embrittlement and its effect on fatigue crack propagation in IN718 at 650°C, Procedia Struct. Integr. 2 (2016) 557–564, https://doi.org/10.1016/j.prostr.2016.06.072.
[138] W. Dietzel, M. Pfuff, G.G. Juilfs, Studies of SCC and hydrogen embrittlement of high strength alloys using fracture mechanics methods, Mater. Sci. Forum 482 (2005) 11–16. https://doi.org/10.4028/www.scientific.net/MSF.482.11.
[139] Z.-H. Hong, S.-F. Hwang, T.-H. Fang, Atomic-level stress calculation and surface roughness of film deposition process using molecular dynamics simulation, Comput. Mater. Sci. 48 (2010) 520–528, https://doi.org/10.1016/j.commatsci.2010.02.018.
[140] M. Rüter, E. Stein, Adaptive finite element analysis of crack propagation in elastic fracture mechanics based on averaging techniques, Comput. Mater. Sci. 31 (2004) 247–257, https://doi.org/10.1016/j.commatsci.2004.03.006.
[141] R.P. Gangloff, Probabilistic fracture mechanics simulation of stress corrosion cracking using accelerated laboratory testing and multi-scale modeling, Corrosion 72 (2016) 862–880, https://doi.org/10.5006/1920.
[142] R. Bashir, H. Xue, J. Zhang, R. Guo, N. Hayat, G. Li, Y. Bi, Effect of material macrostructural parameters on quantitative stress corrosion cracking plastic zone using extended finite element method in welded joints for light water reactor environment, Corrosion 76 (2020) 826–834, https://doi.org/10.5006/3498.
[143] H. Lee, S.J. Kang, J.B. Choi, M.K. Kim, An extended finite element method-based representative model for primary water stress corrosion cracking of a control rod driving mechanism penetration nozzle, Fatig. Fract. Eng. Mater. Struct. 41 (2018) 138–145, https://doi.org/10.1111/ffe.12667.
[144] M. Sedlak, B. Alfredsson, P. Efsing, A coupled diffusion and cohesive zone model for intergranular stress corrosion cracking in 316L stainless steel exposed to cold work in primary water conditions, Eng. Fract. Mech. 217 (2019) 106543, https://doi.org/10.1016/j.engfracmech.2019.106543.
[145] C. Tan, S. Qian, J. Zhang, Crack Extension Analysis of Atmospheric Stress Corrosion Based on Peridynamics, vol. 12, Applied Sciences, 2022, https://doi.org/10.3390/app121910008.
[146] W. Mai, S. Soghrati, R.G. Buchheit, A phase field model for simulating the pitting corrosion, Corrosion Sci. 110 (2016) 157–166, https://doi.org/10.1016/j.corsci.2016.04.001.
[147] C. Cui, R. Ma, E. Martínez-Pañeda, A generalised, multi-phase-field theory for dissolution-driven stress corrosion cracking and hydrogen embrittlement, J. Mech. Phys. Solid. 166 (2022) 104951, https://doi.org/10.1016/j.jmps.2022.104951.
[148] X. Liu, S.-Y. Kim, S.H. Lee, B. Lee, Atomistic investigation on initiation of stress corrosion cracking of polycrystalline Ni60Cr30Fe10 alloys under high-temperature water by reactive molecular dynamics simulation, Comput. Mater. Sci. 187 (2021) 110087, https://doi.org/10.1016/j.commatsci.2020.110087.
[149] A. Hussein, F. Aldakheel, B. Hudobivnik, P. Wriggers, P.-A. Guidault, O. Allix, A computational framework for brittle crack-propagation based on efficient virtual element method, Finite Elem. Anal. Des. 159 (2019) 15–32, https://doi.org/10.1016/j.finel.2019.03.001.
[150] X. Peng, S. Kulasegaram, S.C. Wu, S.P.A. Bordas, An extended finite element method (XFEM) for linear elastic fracture with smooth nodal stress, Comput. Struct. 179 (2017) 48–63, https://doi.org/10.1016/j.compstruc.2016.10.014.
[151] R. Bashir, H. Xue, R. Guo, Y. Bi, M. Usman, Interaction of cyclic loading (Low-Cyclic fatigue) with stress corrosion cracking (SCC) growth rate, Adv. Mater. Sci. Eng. 2020 (2020) 10, https://doi.org/10.1155/2020/8026372.
[152] R. Bashir, H. Xue, J. Zhang, R. Guo, N. Hayat, G. Li, Y. Bi, Effect of XFEM mesh density (mesh size) on stress intensity factors (K), strain gradient ([Formula presented]) and stress corrosion cracking (SCC) growth rate, Structures 25 (2020) 593–602, https://doi.org/10.1016/j.istruc.2020.03.037.
[153] M. Wasim, M.B. Djukic, T.D. Ngo, Influence of hydrogen-enhanced plasticity and decohesion mechanisms of hydrogen embrittlement on the fracture resistance of steel, Eng. Fail. Anal. 123 (2021) 105312, https://doi.org/10.1016/j.engfailanal.2021.105312.
[154] M. Kamaya, T. Haruna, Crack initiation model for sensitized 304 stainless steel in high temperature water, Corrosion Sci. 48 (2006) 2442–2456, https://doi.org/10.1016/j.corsci.2005.09.015.
[155] J. Toribio, F.J. Ayaso, B. González, J.C. Matos, D. Vergara, M. Lorenzo, Critical stress intensity factors in steel cracked wires, Mater. Des. 32 (2011) 4424–4429, https://doi.org/10.1016/j.matdes.2011.03.064.
[156] H. Xue, T. Shoji, Quantitative prediction of EAC crack growth rate of sensitized type 304 stainless steel in boiling water reactor environments based on EPFEM, J. Pressure Vessel Technol. 129 (2006) 460–467, https://doi.org/10.1115/1.2748827.
[157] C. Chen, W. Wang, Z. Zhang, Y. Su, A.A. Volinsky, Cohesive zone modelling of anodic dissolution stress corrosion cracking induced by corrosion product films, Phil. Mag. 99 (2019) 1090–1102, https://doi.org/10.1080/14786435.2019.1575530.
[158] M. Sedlak Mosesson, B. Alfredsson, P. Efsing, Simulation of slip-oxidation process by mesh adaptivity in a cohesive zone framework, Materials 14 (2021), https://doi.org/10.3390/ma14133509.
[159] U. De Francisco, N.O. Larrosa, M.J. Peel, Development of a microstructural cohesive zone model for intergranular hydrogen environmentally assisted cracking, Eng. Fract. Mech. 260 (2022) 108167, https://doi.org/10.1016/j.engfracmech.2021.108167.
[160] N.R. Raykar, S.K. Maiti, R.K. Singh Raman, Modelling of mode-I stable crack growth under hydrogen assisted stress corrosion cracking, Eng. Fract. Mech. 78 (2011) 3153–3165, https://doi.org/10.1016/j.engfracmech.2011.07.013.
[161] L. Fan, Z. Dai, C. Zhang, Z. Yang, H. Chen, Phase field modeling of austenite decomposition and formation in steels: an overview, in: F.G. Caballero (Ed.), Encyclopedia of Materials: Metals and Alloys, Elsevier, Oxford, 2022, pp. 527–540, https://doi.org/10.1016/B978-0-12-819726-4.00117-4.
[162] M. Militzer, 13 - phase field modelling of phase transformations in steels, in: E. Pereloma, D. V Edmonds (Eds.), Phase Transformations in Steels, Woodhead Publishing, 2012, pp. 405–432, https://doi.org/10.1533/9780857096111.3.405.
[163] K. Satake, K. Okada, M. Muramatsu, Phase-field crack analysis using estimated transition zone of crack by molecular dynamics simulation, AIP Adv. 11 (2021) 065206, https://doi.org/10.1063/5.0054236.
[164] J.-Y. Wu, T.K. Mandal, V.P. Nguyen, A phase-field regularized cohesive zone model for hydrogen assisted cracking, Comput. Methods Appl. Mech. Eng. 358 (2020) 112614, https://doi.org/10.1016/j.cma.2019.112614.
[165] T.-T. Nguyen, J. Bolivar, Y. Shi, J. Réthoré, A. King, M. Fregonese, J. Adrien, J.-Y. Buffiere, M.-C. Baietto, A phase field method for modeling anodic dissolution induced stress corrosion crack propagation, Corrosion Sci. 132 (2018) 146–160, https://doi.org/10.1016/j.corsci.2017.12.027.
[166] C. Lin, H. Ruan, Phase-field modeling of mechano–chemical-coupled stress-corrosion cracking, Electrochim. Acta 395 (2021) 139196, https://doi.org/10.1016/j.electacta.2021.139196.
[167] C. Cui, R. Ma, E. Martínez-Pañeda, A phase field formulation for dissolution-driven stress corrosion cracking, J. Mech. Phys. Solid. 147 (2021) 104254, https://doi.org/10.1016/j.jmps.2020.104254.

[168] S. Hirshikesh, R.K. Natarajan, E. Annabattula, Martínez-Pañeda, Phase field modelling of crack propagation in functionally graded materials, Compos. B Eng. 169 (2019) 239–248, https://doi.org/10.1016/j.compositesb.2019.04.003.
[169] B.-H. Choi, A. Chudnovsky, R. Paradkar, W. Michie, Z. Zhou, P.-M. Cham, Experimental and theoretical investigation of stress corrosion crack (SCC) growth of polyethylene pipes, Polym. Degrad. Stabil. 94 (2009) 859–867, https://doi.org/10.1016/j.polymdegradstab.2009.01.016.
[170] D. Kujawski, K. Sadananda, Effect of crack-tip stresses on stress corrosion cracking behavior, Metall. Mater. Trans. 42 (2011) 377–382, https://doi.org/10.1007/s11661-010-0373-5.
[171] D. De Meo, C. Diyaroglu, N. Zhu, E. Oterkus, M.A. Siddiq, Modelling of stress-corrosion cracking by using peridynamics, Int. J. Hydrogen Energy 41 (2016) 6593–6609, https://doi.org/10.1016/j.ijhydene.2016.02.154.
[172] C. Shi, Y. Gong, Z.-G. Yang, Q. Tong, Peridynamic investigation of stress corrosion cracking in carbon steel pipes, Eng. Fract. Mech. 219 (2019) 106604, https://doi.org/10.1016/j.engfracmech.2019.106604.
[173] Z. Chen, S. Jafarzadeh, J. Zhao, F. Bobaru, A coupled mechano-chemical peridynamic model for pit-to-crack transition in stress-corrosion cracking, J. Mech. Phys. Solid. 146 (2021) 104203, https://doi.org/10.1016/j.jmps.2020.104203.
[174] I.B. Obot, K. Haruna, T.A. Saleh, Atomistic simulation: a unique and powerful computational tool for corrosion inhibition research, Arabian J. Sci. Eng. 44 (2019) 1–32, https://doi.org/10.1007/s13369-018-3605-4.
[175] G. Szefer, D. Jasińska, Modeling of strains and stresses of material nanostructures, Bull. Pol. Acad. Sci. Tech. Sci. 57 (2009) 41–46, https://doi.org/10.2478/v10175-010-0103-6.
[176] Q.K. Li, Y. Zhang, W.Y. Chu, Molecular dynamics simulation of stress corrosion cracking in Cu3Au, Comput. Mater. Sci. 25 (2002) 510–518, https://doi.org/10.1016/S0927-0256(02)00328-2.
[177] Y.-A. Zhang, J. Tao, X. Chen, B. Liu, Mixed-pattern cracking in silica during stress corrosion: a reactive molecular dynamics simulation, Comput. Mater. Sci. 82 (2014) 237–243, https://doi.org/10.1016/j.commatsci.2013.09.045.
[178] M.S.R. Elapolu, A. Tabarraei, An atomistic study of the stress corrosion cracking in graphene, J. Phys. Chem. A 124 (2020) 7060–7070, https://doi.org/10.1021/acs.jpca.0c04758.
[179] N.K. Das, K. Suzuki, Y. Takeda, K. Ogawa, T. Shoji, Quantum chemical molecular dynamics study of stress corrosion cracking behavior for fcc Fe and Fe–Cr surfaces, Corrosion Sci. 50 (2008) 1701–1706, https://doi.org/10.1016/j.corsci.2008.01.032.
[180] S. Kotsiantis, Supervised machine learning: a review of classification techniques, Informatica 31 (2007) 249–268.
[181] A.I. Kadhim, Survey on supervised machine learning techniques for automatic text classification, Artif. Intell. Rev. 52 (2019) 273–292, https://doi.org/10.1007/S10462-018-09677-1.
[182] H.A. Al-Jamimi, S. Al-Azani, T.A. Saleh, Supervised machine learning techniques in the desulfurization of oil products for environmental protection: a review, Process Saf. Environ. Protect. 120 (2018) 57–71, https://doi.org/10.1016/j.psep.2018.08.021.
[183] A.H. Alamri, Application of machine learning to stress corrosion cracking risk assessment, Egyptian Journal of Petroleum 31 (2022) 11–21, https://doi.org/10.1016/j.ejpe.2022.09.001.
[184] N. Narimani, B. Zarei, H. Pouraliakbar, G. Khalaj, Predictions of corrosion current density and potential by using chemical composition and corrosion cell characteristics in microalloyed pipeline steels, Measurement 62 (2015) 97–107, https://doi.org/10.1016/j.measurement.2014.11.011.
[185] Z. Fan-Zi, Q. Zheng-Ding, A survey of classification learning algorithm, in: Proceedings 7th International Conference on Signal Processing, ICSP '04, 2004.
[186] M. Smith, A. Blenkinsop, M. Capewell, B. Kerrigan, Now you SCC me, now you don't: using machine learning to find stress corrosion cracking, International Pipeline Conference (2020), https://doi.org/10.1115/IPC2020-9624.
[187] G. Hinton, T.J. Sejnowski, Unsupervised Learning: Foundations of Neural Computation, MIT Press, The, 1999, https://doi.org/10.7551/mitpress/7011.001.0001.
[188] N. Li, M. Shepperd, Y. Guo, A systematic review of unsupervised learning techniques for software defect prediction, Inf. Software Technol. 122 (2020) 106287, https://doi.org/10.1016/J.INFSOF.2020.106287.
[189] I. Goodfellow, Y. Bengio, A. Courville, Deep Learning, MIT Press, The, 2016.
[190] Y. LeCun, Y. Bengio, G.E. Hinton, Deep learning, Nature 521 (2015) 436–444, https://doi.org/10.1038/nature14539.
[191] J. Schmidhuber, Deep learning in neural networks, Neural Network. 61 (2015) 85–117, https://doi.org/10.1016/J.NEUNET.2014.09.003.
[192] D.E. Rumelhart, G.E. Hinton, R.J. Williams, Learning representations by back-propagating errors, Nature 323 (1986) 533–536, https://doi.org/10.1038/323533a0.
[193] M. Aslam, J.-M. Lee, S. Hong, A multi-layer perceptron based deep learning model to quantify the energy potentials of a thin film a-Si PV system, Energy Rep. 6 (2020) 1331–1336, https://doi.org/10.1016/j.egyr.2020.11.025.
[194] W. Rawat, Z. Wang, Deep convolutional neural networks for image classification: a comprehensive review, Neural Comput. 29 (2017) 2352–2449, https://doi.org/10.1162/NECO_A_00990.
[195] T. Papamarkou, H. Guy, B. Kroencke, J. Miller, P. Robinette, C.S. Schultz D, Automated detection of corrosion in used nuclear fuel dry storage canisters using residual neural networks, Nucl. Eng. Technol. 53 (2021) 657–665, https://doi.org/10.1016/j.net.2020.07.020.
[196] M. Schuster, K.K. Paliwal, Bidirectional recurrent neural networks, IEEE Trans. Signal Process. 45 (1997) 2673–2681, https://doi.org/10.1109/78.650093.
[197] Z. Li, Y. Lu, X. Wang, Modeling of stress corrosion cracking growth rates for key structural materials of nuclear power plant, J. Mater. Sci. 55 (2020) 439–463, https://doi.org/10.1007/s10853-019-03968-w.
[198] A. Creswell, T. White, V. Dumoulin, K. Arulkumaran, B. Sengupta, A.A. Bharath, Generative adversarial networks: an overview, IEEE Signal Process. Mag. 35 (2018) 53–65, https://doi.org/10.1109/MSP.2017.2765202.
[199] S. Hochreiter, J. Schmidhuber, Long short-term memory, Neural Comput. 9 (1997) 1735–1780, https://doi.org/10.1162/NECO.1997.9.8.1735.
[200] C. Xinyu, Z. Yingbo, L. Jiaheng, C. Hui, Composition design of 7XXX aluminum alloys optimizing stress corrosion cracking resistance using machine learning, Mater. Res. Express 7 (2020) 46506, https://doi.org/10.1088/2053-1591/ab8492.
[201] H.M. Smets, W.F. Bogaerts, SCC analysis of austenitic stainless steels in chloride-bearing water by neural network techniques, Corrosion 48 (1992) 618–623, https://doi.org/10.5006/1.3315981.
[202] Giulia De Masi, Roberta Vichi, Manuela Gentile, Roberto Bruschi, A neural network predictive model of pipeline internal corrosion profile, in: 2014 First International Conference on Systems Informatics, Modelling and Simulation, IEEE, 2014, pp. 18–23.
[203] G. Qian, K. Tantratian, L. Chen, Z. Hu, M.D. Todd, A probabilistic computational framework for the prediction of corrosion-induced cracking in large structures, Sci. Rep. 12 (2022) 1, https://doi.org/10.1038/s41598-022-25477-8.
[204] A. Dourado, F.A.C. Viana, PHYSICS-INFORMED neural networks for corrosion-fatigue prognosis, in: Annual Conference of the, PHM Society, 2019, pp. 1–12.
[205] J. Spanner, L. Udpa, R. Polikar, P. Ramuhalli, Neural Networks for Ultrasonic Detection of Intergranular Stress Corrosion Cracking, vol. 409, American Society of Mechanical Engineers, Pressure Vessels and Piping Division (Publication) PVP, 2000, pp. 215–221.
[206] S.A. Lajevardi, T. Shahrabi, V. Baigi, S.M. A, Prediction of time to failure in stress corrosion cracking of 304 stainless steel in aqueous chloride solution by artificial neural network, Protect. Met. Phys. Chem. Surface 45 (2009) 610–615, https://doi.org/10.1134/S2070205109050207.